Department of Machine Elements
Mechanical Engineering Sciences

ISRN: LUTMDN/TMME—5008—SE

Design of a dry clutch testing rig for emission studies

Master's Dissertation by

Driton Sabani and Isa Yenibayrak

Supervisor:
Doctoral student and Lecturer, Rikard Hjelm, Division of Machine Elements

Examiner:
Professor, Jens Wahlström, Division of Machine Elements

Abstract

Air pollution in European cities due to the transport sector is still threatening to human health. Most dry clutch systems used in passenger cars are not completely sealed off from the environment, and thus a potential source to pollution. The mapping of this pollution is not readily available compared to other systems, such as brake systems, and therefore research regarding the topic is wanted.

As a part of the European Union nPETS-project, this thesis work aims to develop a test rig where particles can be measured under controlled circumstances. An electric motor will drive a friction disc, which will be in a slip contact against metal surfaces. The motor will be part of an thermal analysis, where the power output from the motor will be evaluated. The clutch assembly will be sealed off from the surrounding environment and the airflow will be controlled by a filtered inlet and monitored outlet, as per instructions. The encapsulation will be designed by the help of CFD-simulations. The simulations will help determine the design of the encapsulation and propose an inlet airspeed. Clutch engagement dynamics will be studied, and the slip time in the test rig will be related to a real-life engagement. The particles will be directed towards an outlet, where they in future works can be collected and measured.

Contents

Acronyms

CFD Computational Fluid Dynamics.

EM Electrical Motor.

EU European Union.

FD Friction Disc.

FEM Finite Element Method.

HEPA High Efficiency Particulate Arresting.

ICE Internal Combustion Engine.

nPETS Nanoparticle Emissions from the Transport Sector.

OEM Original Equipment Manufacturer.

RPM Revolutions Per Minute.

1 Introduction

1.1 Background

Particles emitted from the transport sector can be divided into two main categories, exhaust and non-exhaust emissions. Non-exhaust emissions from passenger vehicles has predominantly been focused on brake and tyre emissions [1] [2]. Less literature is found on dry clutch emissions, where Jacko et al. [3] is one of few. As of 2014, dry clutch transmissions are one of the most common types of transmissions in a passenger vehicle [4].

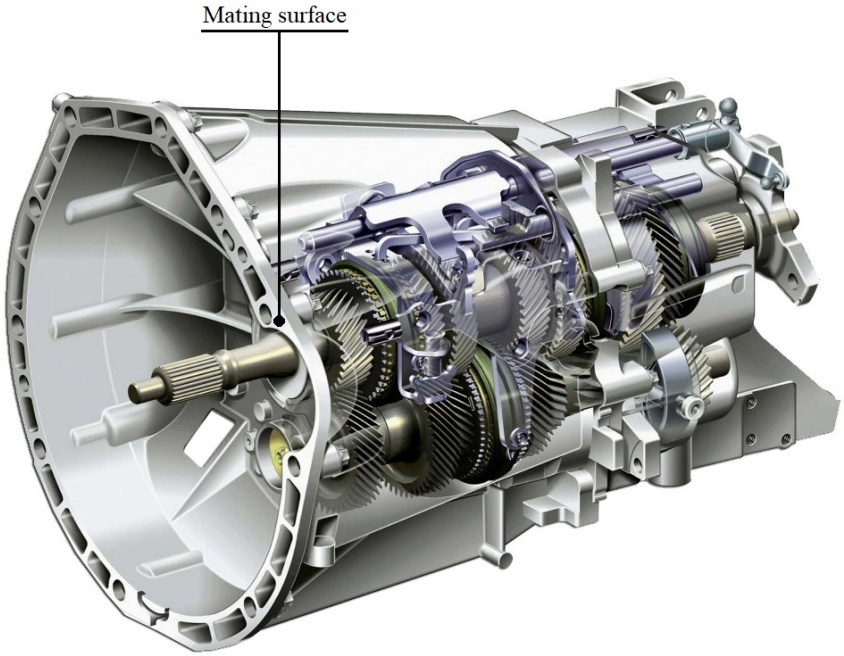

Figure 1: *Gearbox housing, mating surface marks potential crevices, figure adapted from [5]*

Clutches are worn down, primarily abrasively [3] due to *slip*, which essentially occurs when the input and output shafts does not have the same rotational speed. Throughout this wear, particles are generated and released to the surrounding gearbox housing. The mating surface in figure 1 is in most cases directly bolted against a combustion engine, with or without a seal depending on manufacturer and thereby a potential leak source. To be able to measure if this leak source is substantial, and possibly existent at all, a testing rig that allows a controlled environment is to be designed.

Most European cities are filled with vehicles that contribute to air pollution and thus potential adverse health effects to human life. The aim of this thesis is to aid and fill the research gap in emissions related to dry clutch systems in passenger vehicle, as part of the nPETS project. It is so far unclear if dry clutch emissions get airborne and thus are harmful. Depending on the outcome, further investigation might be necessary since the project's aim is to determine whether the problem exists or not.

The nPETS project is an ongoing project created and founded by the EU. It is coordinated by KTH Royal Institute of Technology, and contributed by Lund University, amongst others. The aim of nPETS project is to study the characteristics of sub 100 nm particles emitted from the transport sector, including passenger cars, and its potential effects on human and animal life [6]. Dry clutch emissions are thus a part of the project, and will be investigated. This thesis will aid the research on non-exhaust emissions from passenger vehicle dry clutch systems.

1.2 Problem description

As a contribution to the nPETS project a testing rig is to be designed and constructed, where particle samples can be generated and probably measured and collected in the future. It's not a part of the thesis to collect particles, nor draw conclusions from the effect of particles.

1.3 System overview

Figure 2 presents a simple overview of the testing rig. The shaft which is connected to an electrical motor will rotate the friction plate which slips against a contact surface to induce wear. The clutch system will be encapsulated by a box which represents a typical transmission housing with its corresponding seal. A second encapsulation which represents the atmosphere encapsulates the transmission housing. As per instructions, the inlet will consist of a fan and a HEPA-filter to ensure that uncontaminated air enters the sealed box, the measurements will be taken at the outlet sampling point, where a particle counter will be installed.

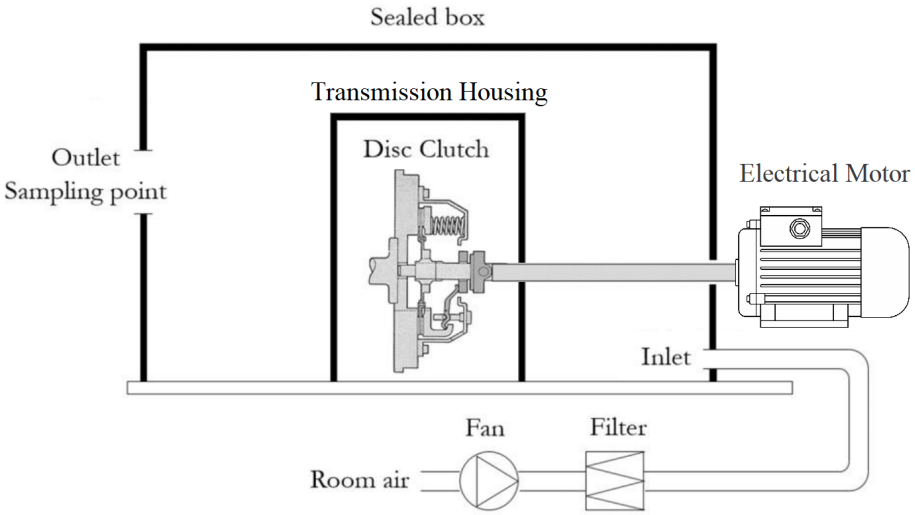

Figure 2: *Testing rig system overview*

1.4 Objectives

The aim of this thesis was to develop a testing rig which will be used to generate particles by slipping a clutch under controlled circumstances. By controlled circumstances, the slip speed, clutch temperature and the ability to measure particles is considered. The testing rig should be easy to operate and modular which makes it possible to change friction plates without completely disassembling the testing rig. The underlying research question of this thesis is proposed as":

"How can a testing rig be designed such that it can slip a clutch under controlled circumstances?"

Some additional targets can be expressed as:

- An inlet airspeed should be proposed.
- The ease of changing friction plate should be considered.

1.5 Limitation

To be able to complete the thesis in the limited time span certain limitations were set, these limitations are presented in the following bullet point list:

- The thesis was limited to design and construct a testing rig. If time allows, initial particle samples will be taken with a supervisor. The potential research samples will not be handled in this thesis.
- The testing rig will be designed with in mind so most standard dry clutches from modern passenger cars can be used by making smaller modifications to the testing rig. This allows for different clutch materials to be tested, however, initially only the selected clutch model can be guaranteed to work in the testing rig.
- Only the crevices facing the combustion engine will be considered as a potential leak source. The pathway through the gearbox is less likely to release particles into the atmosphere, since the gears are covered in oil which is more likely to trap particles.

1.6 Literature study

A literature study was carried out to find relevant information surrounding the project, and as a consequence motivate the project. Clutch emission generation is relatively unknown, where one of few papers considering clutch emissions is Jacko et al.[3]. In that case, the gearbox housing does have holes, some of which were sealed, and others used as an inlet and outlet. This implies that the escape process dynamics are not taken into account. Instead particle measurements are taken as generated by the clutch, and the "airborneness" is estimated. Moreover, clutch temperatures are not monitored, and the dynamics of a clutch engagement is not expressed since the particle samples are taken from a real vehicle. For further education about the engagement process, Pisaturo et al.[7] is used. Hard engagements are simulated, where friction coefficients, power and heat fluxes are estimated. It is seen that an engagement process generates approximately 35kJ of heat energy, with a peak power of 25kW, while the torque produced from the engine can be regarded as a common vehicle. Wear of friction material is not considered in this paper. It is also an reasonable assumption to estimate the released nano-particles to follow air streamlines, as supported by Wang et al. [8], which will be an assumption used in the CFD-simulations. It seems clear that there is a motive to fill the research gap regarding clutch wear, and how seals affect the particle released.

2 Methodology

2.1 Clutch system

A clutch system is a machine element which connects or disconnects two rotating shafts through friction, the forces and movements acting on the shafts are transferred without a change in magnitude through the construction [9]. This thesis will only cover dry lamella clutches, where the transmitted forces and movements are made via friction, but compared to a wet clutch a dry clutch does not sit in an oil bath and is thereby denoted as "dry" [10]. This type of clutch is the only focus of the thesis work, since the lack of lubricant liquid allows for particles to follow air streams, potentially out into the atmosphere, which is the investigation objective following the design of the testing rig.

2.1.1 Dry clutch system

Figure 3 presents a typical dry clutch configuration in an exploded view. The clutch cover containing the pressure plate and diaphragm spring is bolted against the flywheel, clamping the friction plate in between. Notice that not all friction plates are symmetrical, but rather has the sprung centre containing the cushion springs extruded in one direction. In an unloaded state, the clamping force is at its highest. When the clutch pedal in a manual transmission vehicle is depressed, the release fork applies force on the diaphragm spring via the throw-out bearing which makes the pressure plate retract, effectively disconnecting the engine from the gearbox since the friction plate no longer is clamped between the flywheel and the pressure plate .

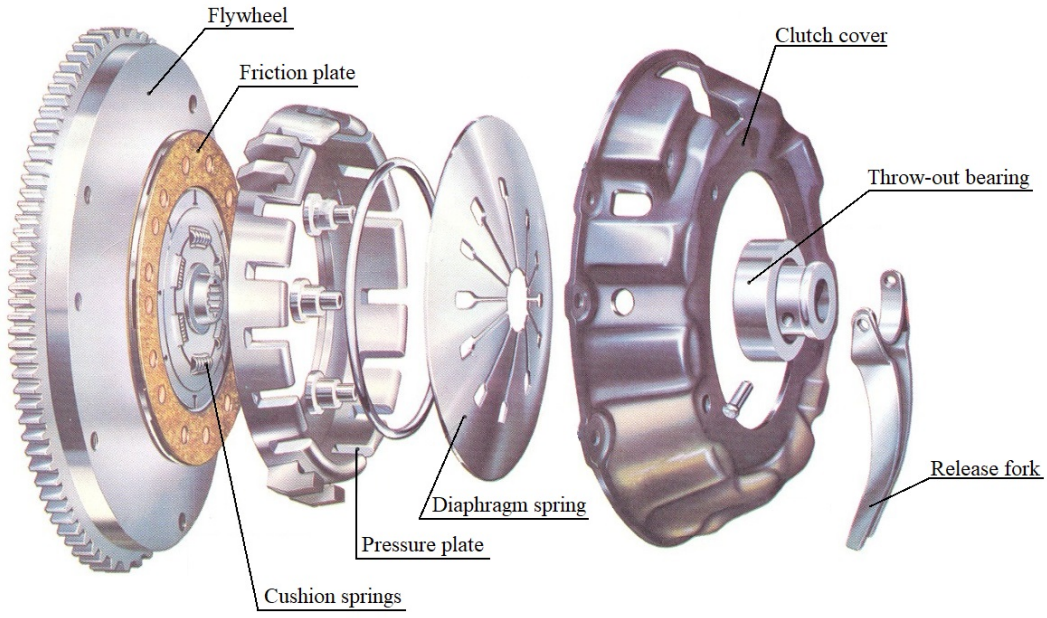

Figure 3: *Exploded view of a diaphragm dry clutch system, figure adapted from [5]*

2.1.2 Engagement process

A running combustion engine in a vehicle that is not in motion is labeled *idle*. In this state no torque is transferred though the clutch and there is no connection between the engine and wheels. To propel the vehicle, a gear is selected and the clutch is engaged by releasing the clutch pedal. This axially loads the clutch, creating a clamping force. Equation 2.1 states that the clamping force is proportional to the maximum transferable torque.

$$M = \mu n \int_{R_i}^{R_y} p 2\pi r^2 dr = \mu n F \frac{R_i + R_y}{2} [9] \tag{2.1}$$

Where M is the maximum transferable torque, μ is the friction coefficient between the friction plate and pressure plate contact surface, n the number of contact surfaces, F is the clamping force and $R_i \& R_y$ the inner and outer radii, respectively.

During an engagement, there is a dynamic relationship in the rotational speed between the engine (flywheel) and wheels (friction plate). This phenomena is called *slip*, and is the primary reason for the abrasive wear in a clutch. The slip velocity was chosen according to [7], which states an average slip speed of approximately 100 rad/s during a fast acceleration from standstill.

According to Pisaturo et al. [7], slipping the clutch during a three second engagement process can induce thermal power peaks of over 25kW. This heat is generated in the contact surfaces between the flywheel, friction plate and the pressure plate. This results in a total clutch temperature rise of 30°C, generating approximately 35kJ of heat energy during an engagement. Since the engagement processes might vary, this information can be useful to compare different scenarios.

2.1.3 Friction material

A typical passenger car friction plate is laminated with a friction material. There are several types of friction materials which can be used in a passenger vehicle application, where the most common OEM is an organic material [11], and will thus be the chosen material for this thesis work. According to data-sheets for a typical engineering application organic friction material, the dynamic coefficient of friction is only slightly varying in the temperature range of 50 to 250°C [12], which is also assumed to be the working range. According to [7], the friction coefficient of the material does vary with contact pressure, temperature and slip speed [13].

In addition to being long lasting, a friction plate is characterized by the follow criteria:

- Able to transfer a specific torque at a certain RPM.
- Manage the heat from many engagements.
- Withstand the clamping force.

It's clear that different manufacturers achieve the above criteria in different ways, with different material compositions, which can affect the particle generation. Once again, this will not be considered in this thesis, but is a factor when further evaluating particle generation.

2.2 Slip process

There are two main methods of operating slip in a testing rig. One is similar to the application in a road vehicle, where the slip occurs occasionally but with considerable power and large temperature derivatives. The temperature is then controlled by periodically slipping by engaging and disengaging the clutch. Accurate control is needed, since the clutch temperature can increase by tenths of degrees from a few seconds of slip.

The other method is a continuous slip engagement where the power is relatively limited, and where the temperature derivative eventually reaches zero at a desired temperature. This method is less complex and requires less control if designed properly.

The design of the testing rig is greatly dependant on which type of slip operation is chosen. This is since every major component has to be dimensioned with respect to the contrasting acting forces. Table 1 presents the advantages and disadvantages with the respective method.

	Periodic slip	**Constant slip**
Control of slip	-	+
Input torque	-	+
Rig agility	-	+
Control of temperature	-	+
Particle sampling	-	+
Realistic contact pressure	+	-
Realistic wear and temperature	+	-
General realism	+	-

Table 1: *Comparison between concepts for slip*

Judging on table 1, it seems that the constant slip method is the more versatile concept. It implies no external control, lower torque, a lighter construction, easy temperature control and should induce wear particles at a constant rate, which should make sampling easier. The periodic slip concept provides realism, but the scale of the project is completely different and requires heavy-duty equipment. Moving forward, the *constant slip* method is chosen as the method of choice.

2.3 Concept

The following section describes initial design concepts and choices for different subsystems. Note that the design choices run in parallel. For example, the setup for the thermal analysis of the clutch used input data from the EM. Moreover, the setup for the thermal and CFD-analysis are explained. The subsystems are split into the following subsections:

- Frame
- Clutch assembly
- Electric motor
- Encapsulation
- Data sampling

2.3.1 Frame

System requirement

The frame establishes the foundation of the design. It should be able to support the EM and clutch assembly during operation, it should also allow the encapsulation to utilize its design to seal the clutch assembly in an effective way.

Concept

Initially, a design with the opportunity to run both constant and periodic slip was investigated. The goal of the initial prototype was to imitate the mating surface between a real gearbox housing and a combustion engine, where the metal to metal contact surface could represent reality.

Due to constraints in the project, an existing frame was offered which is presented in figure 4. The frame has previously been used for a similar application. After evaluating the frame in regards to the dimensions and structural integrity, it was concluded that the frame could be reused and would only require some minor modifications.

Frame integrity analysis

FEA was used to validate the structural integrity of the frame, the method and results from the FEA can be found in Appendix A section A1. In short, as anticipated the frame is well overdimensioned for the acting forces and can be used with no risk for failure.

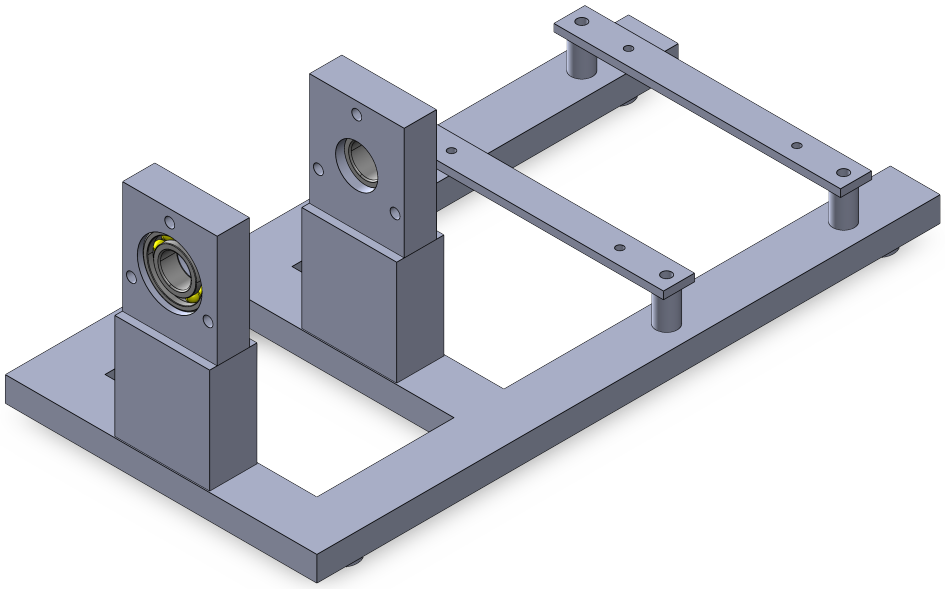

Figure 4: *Original frame assembly.*

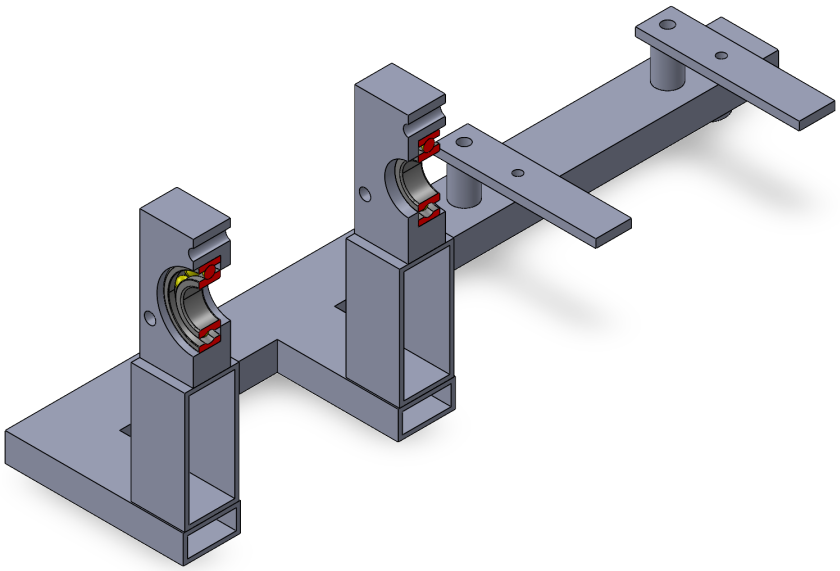

Figure 5: *Section view of original frame assembly, the frame mainly consists of welded rectangular steel tubes with 3mm wall thickness.*

2.3.2 Clutch assembly

System requirement

The clutch system should be commonly found in a European passenger vehicle and the friction pads must be made of an organic material. The friction plate in its original design should be subjected to similar clamping forces on both sides. Due to the design of the frame, it's beneficial if the clutch assembly is lightweight. Neither the friction plate or pressure plate can have an outer diameter exceeding 300mm since there will be interference with the frame.

Choice of clutch

The choice of clutch is made with regards to the goal of the project, in essence, choosing a clutch which can represent a commonly found passenger vehicle on European roads. The average age of a passenger vehicle in Europe is 11.5 years old [14]. Although there are some models which are dominant by means of number of sales on the market, there is no suggesting that these cars fall under the category relevant to our project. In other words, neither the engine or the transmissions type are specified and thus one can only have an educated guess on which clutch assembly is used. Out of probability, the VAG Group produces cars under the name of many car brands and have done so for years on end, including Volkswagen, Audi, Seat, Skoda etc. Most of these brands share the same powertrain system and thus the same manual gearbox. Being amongst the top selling cars for many years [15], it's reasonable to assume that a dry clutch system found in, amongst other models, a Volkswagen Golf, is one of the most common. Furthermore, judging from the top five selling vehicles, the average weight is approximately 1400kg. Moreover, most of the passenger cars in use in the EU use a petrol engine [16]. The average engine cubic capacity and engine power for new passenger cars registered in the last 30 years has been approximately 1.6l and 85kW.

Age	11.5 years [14]
Weight	1400 kg
Engine displacement	1.6 L [17]
Maximum power output	85 kW [17]

Table 2: *Average EU vehicle specification.*

Our choice is guided by the above stated facts, but also of how many models the powertrain system are found in. Our choice is a 220mm clutch assembly found in manual transmission vehicles manufactured between year 1997 - 2020 which is delivered with a 1.6L 75kW engine from VAG Group. The Volkswagen Golf have utilized this clutch assembly amongst many others car models which are listed in Appendix A section A2.

Clutch assembly modifications

Since the *Constant slip* concept was chosen the original clutch assembly will be modified in order to suit the new concept. The clutch assembly in it's original form is heavy and the diaphragm spring constant is very high. For this reason the pressure plate seen in figure 6 was separated from the clutch cover by removing the rivets which holds the assembly together. This results in overall reduced system mass which reduces the frictional forces on the slider pins seen in figure 19, this also allows the clutch system to reach its operating temperature in a shorter amount of time.

Furthermore, the task of the flywheel is replaced with another pressure plate on the grounds that the simplicity and weight is reduced without a compromise in accuracy, rather the opposite due to the advantages of the symmetry.

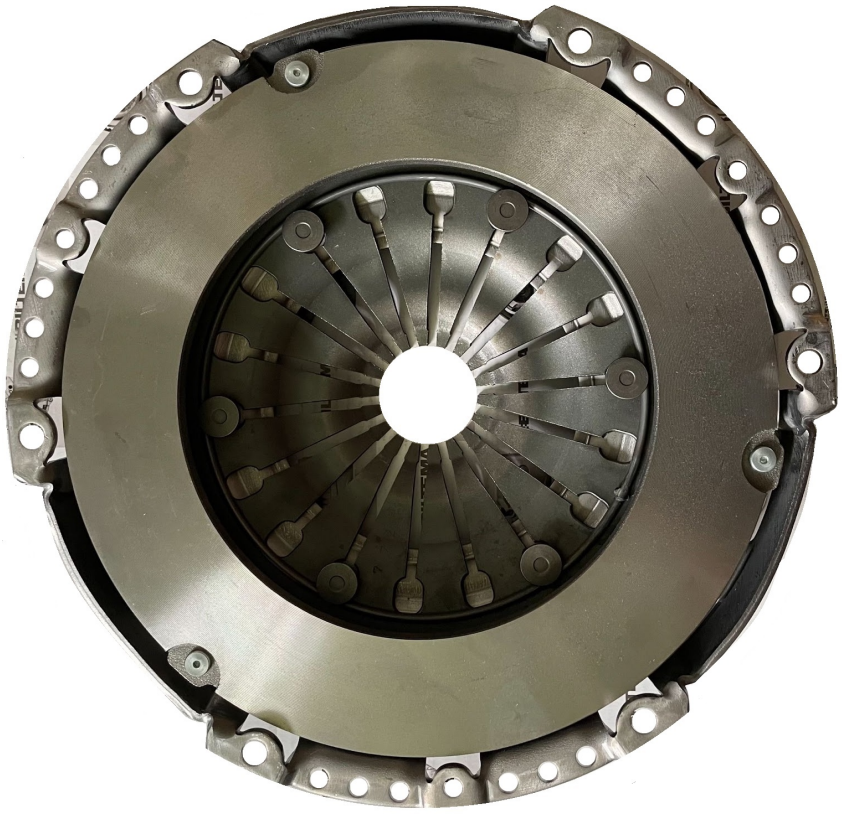

Figure 6: *Original clutch assembly.*

Pressure plate holder

Since the pressure plate was removed from the clutch cover, a pressure plate holder was designed in order to hold the pressure plate in place. The holder also allows the drive shaft to go trough its center and acts as a fastening point for the slider pins. A set of aluminium spacers have been added between the pressure plate and the holder, the backside of the pressure plate can't in a secure way be mounted directly against the holder, instead the rivet holes together with the spacers are utilized for fastening. Effectively the heavy original clutch cover has been replaced by a 5mm thick laser cut aluminium plate.

Friction plate shaft

Generally a splined shaft is used when torque is transferred from the friction plate to the gearbox input shaft as seen in figure 1, this allow high torque to be transferred without risk for slip. However, spline cutting is complex and the fact that the low torque *Constant slip* concept is chosen, the splines in the friction plate was not utilized for torque transfer between the EM and the friction plate.

The EM which rotates the friction disc is substantially weaker than the ICE utilizing this clutch assembly and produces $<$2.5Nm. Instead a shaft utilizing clamping forces is designed where a 6mm threaded rod together with a nut is used to clamp the two shafts to the friction plate. This mounting method is applicable for clutches from other manufacturers as well, since the spline dimension is standardized for this model of clutch assembly.

Force application

The mounting method for the clutch assembly in this construction, differs compared to the to the mounting method in a car where the clutch cover together with the pressure plate and diaphragm spring is bolted against the flywheel. Since this construction lacks a flywheel and as established earlier, that the original diaphragm spring used in the original clutch assembly has a high spring constant, it's not usable for this construction.

Instead, a total of three springs for each pressure plate are used to apply evenly distributed force over the pressure plate clamping the friction plate in between. These springs are mounted in a way which allows each pressure plate to independently move in the axial direction, and will ensure that the pressure plates has contact with the friction disc under all times. It's possible to alter the contact pressure by adding a shim between the spring and bearing holder, this will effectively change the pretension of the spring and thereby the clamping force

By using this method compared to using a fix axial position, it's also ensured that the contact pressure between the friction plate and the pressure plate is near constant even when wear occurs from slip.

Spring constant

To determine the size of the spring constant, equation 2.1 was rewritten and the following calculations and assumptions were made.

$$F = \frac{M}{\mu n \frac{R_i + R_y}{2}} \tag{2.2}$$

The torque M is estimated to 0.38Nm according to figure 8 and the friction coefficient μ is estimated to 0.33 according to [12]. The number of contact surfaces n is set to two. This results in a clamping force of approximately 7N. Adding the fact that there is friction between the slider pins and the bearing holders, springs with a spring constant of 2.6 N/mm are chosen. The springs are pretensioned 1mm by default, resulting in a axial force of 15.6N. As mentioned, this axial force can be altered by further compressing the springs via shims.

2.3.3 Electric motor

System requirement

The EM should be able to slip the clutch to induce heat and wear. The EM should also be able to overcome the maximum transferable torque from the clutch assembly while rotating at approximately 100rad/s according to 2.1.2. A temperature in the range above 50°C and lower than 250°C should be maintained as established in 2.1.3. It's also beneficial to control the slip speed and power input without an external control system. Furthermore, the EM has to fit within the frame dimensions.

Thermal analysis

An existing EM which was included with the frame was evaluated. The motor does fit the frame dimensions, and has been previously used for similar applications. A thermal analysis was made based on the motor specification, to ensure that the power output from the EM is sufficient to achieve the specified clutch temperature range. The friction heat power was estimated as a heat power that is split between the friction plate and the pressure plate. The heat is then conducted to the pressure plate holder. The heat convection coefficients and remaining thermal loads for the different surfaces are chosen according to [18], and are presented in table 3. Material properties are presented in Appendix A section A3.

The meshing is presented in figure 7. It consists of 123589 elements and 206338 nodes, with an element size of 0.7-3.5mm. Only half of the symmetric clutch was modeled, and thus half of the max heat power is generated in the friction surface. The ambient temperature is approximated to 40°C, when accounting for the encapsulation. Note that there is no rotational velocities in this simulation.

	Convection $[\frac{W}{m^2K}]$	**Heat power** $[W]$	**Thermal resistance** $[\frac{K}{W}]$
Friction plate rims	64		
Pressure plate holder	21		
Pressure plate	16		
Contact surface		92.5	$9 \cdot 10^{-5}$

Table 3: *Thermal loads and contact sets for the clutch thermal analysis.*

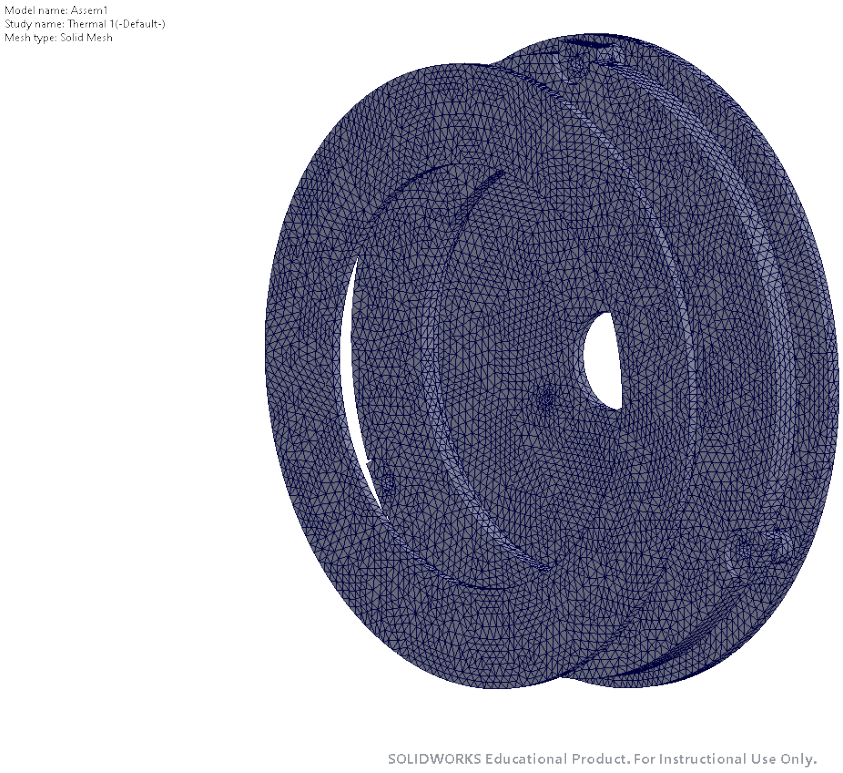

Figure 7: *Prepared mesh for the thermal analysis.*

Multifix MR 25

The Multifix MR 25 EM is a single-phase repulsion induction motor with a power output of 185W and built in speed control. The benefit of using this type of motor is it's high starting torque for a given current draw [19]. In this case, it will help overcome the higher static friction force when initiating the slip process from standstill. The rotating speed and torque can be adjusted by changing the position on a lever located on the back of the motor. This lever effectively changes the input power to the slipping clutch which eventually determines the temperature and the relative slip speed.

The provided Speed-Torque diagram for the Multifix MR 25 EM which is presented in figure 8 indicates a maximum specified torque of 0.38 Nm at a brush angle between 40^{o} - 60^{o}. However, after initial testing, it's clear that the maximum torque output from the EM is well over the specified value and occurs at maximum brush angle.

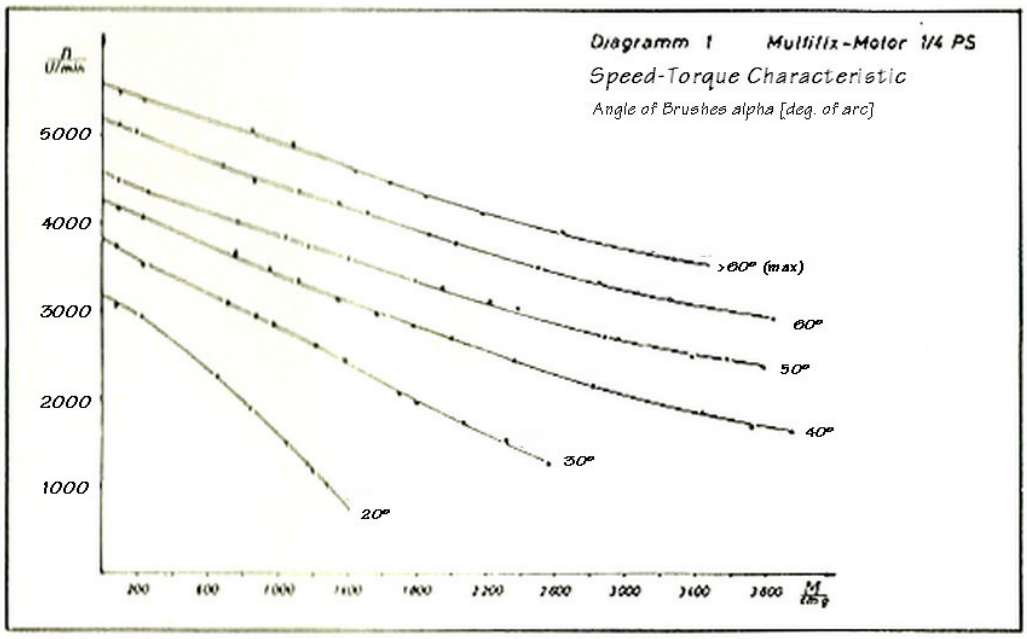

Figure 8: *Multifix Record MR 25 Speed-Torque Characteristics.*

For verification purposes, the following test was conducted, a simple leverage setup seen in figure 9, consisting of a 500mm symmetric lever was used. The lever is connected through it's center of gravity to the center-point of the output shaft from the EM. By using this setup, no torque will act on the shaft in it's unloaded state, which is desired when taking torque measurements.

By letting the lever push on a accurate scale the maximum torque output could be calculated. As anticipated it was concluded that the maximum torque output was much higher compared to the stated value.

By studying the Speed-Torque diagram in figure 8 we can obtain that none of the curves reaches the speed zero at their declared maximum torque. This suggest that the diagram does not specify the entire operating spectrum of the EM and thus explain the low suggested maximum torque output.

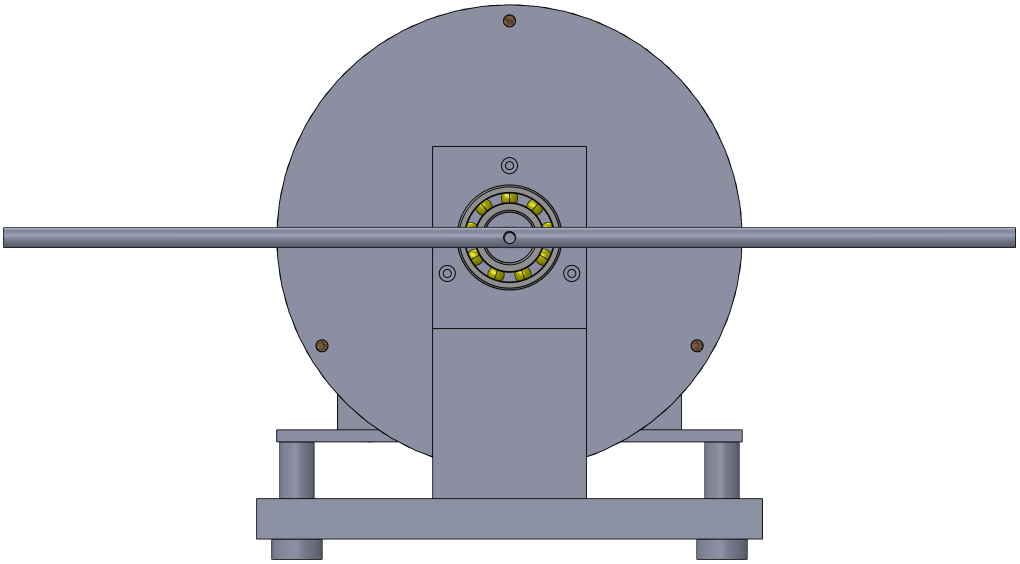

Figure 9: *Leverage setup for torque measurement.*

Since the EM is intended to be used at speeds close to 100rad/s, the provided diagram from the manufacturer has to be extended for the maximum brush angle. This was done by using a set of springs with a know spring constant combined with the symmetrical lever. The springs pretension where increased from 1-4mm in three steps, the rotational speed of the friction disc and the required torque to initiate and maintain slip where measured for each step, this made it possible to calculate both the static and dynamic friction coefficients using a rewritten from of equation 2.1.

2.3.4 Encapsulation

System requirement

The purpose of the encapsulation is to ensure a reliable sampling environment. The particles released should be directed towards a sampling point. The ease of changing the type of seal between the simulated gearbox housing and atmosphere is also taken into account. It should also be possible to access the friction plate without completely disassembling the encapsulation.

CFD simulation

A setup of the encapsulation is modeled and used to simulate the airflow. It's assumed that the particles of interest, due to their size and weight, enters and follows streamlines [8] caused by an inlet fan and the disturbances caused by the rotating friction plate. To determine an initial design and ensure that the simulation is correctly setup, only the outer box is simulated. Continuing, the design process flowchart can be seen in figure 10.

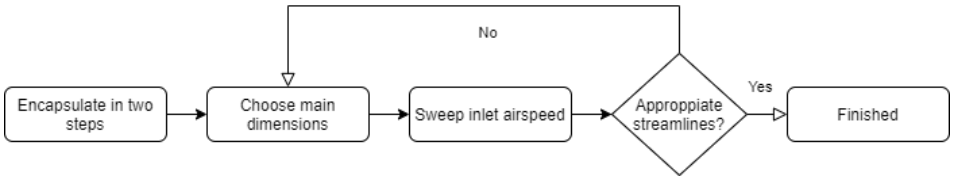

Figure 10: *Design process for the encapsulation.*

In the first steps, a design including an inner and outer encapsulation with appropriate dimensions are chosen. Three inlet speeds are swept in the sweep process to ensure suitable velocity vectors. By suitable, the following points are considered:

- The airflow should , if at all, only be allowed to get trapped to a minimal extent.
- Airflow should not move uninterfered from inlet to outlet, in other words, the air must get entangled with the inner box.
- Volume flow to the inner box.

The above stated points will be rated by observing and rating velocity vectors based on appearance. Similar simulation setup settings are used throughout the process, with the addition of cell zone conditions when the rotating friction plate is added. The turbulence model used is the *realizable k-epsilon* model, with the near-wall treatment as a *scalable wall function*. The cell zone conditions is applied for the rotating friction plate as a frame motion, with a rotational velocity of 100rad/s.

Firstly, a steady state simulation is made for the outer box. The mesh can be seen in figure 11. The element size is set to 20mm, which resulted in 8809 nodes and 42958 elements. The inlet is designed for fan measuring 100mm in diameter, and the swept airflow corresponds to $0.79 - 4.71 \frac{dm^3}{s}$. Every simulation is iterated for 1500 iterations.

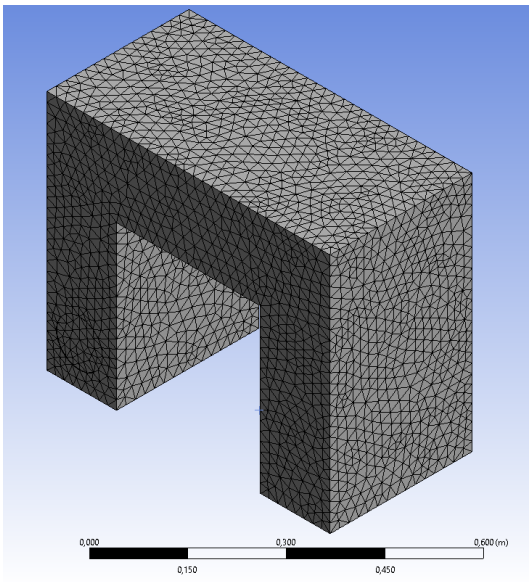

Figure 11: *Mesh of outer box.*

Continuing, a rotating friction plate is added together with the inner box. Initially no top lid is added to ensure that the rotating disc does affect the airflow, see figure 12. Similar mesh size is used for the inner box, with an denser mesh for the rotating friction plate, an element size of 9mm results in 23987 nodes and 115997 elements.

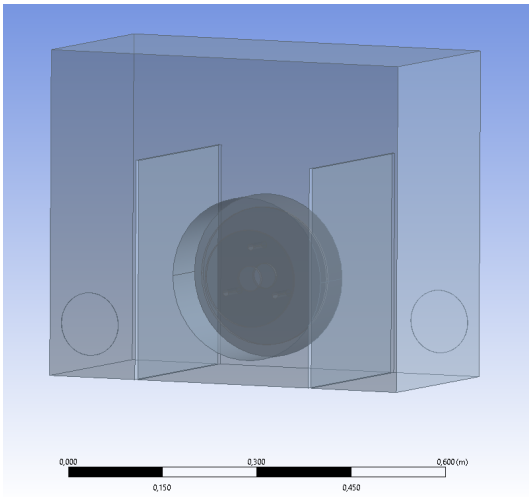

Figure 12: *Transparent geometry, no lid.*

Moreover, to determine the entanglement, the ratio between the volume flow through a plane that is the border between the inner and outer box will be compared to a plane that measures the flow through the top section, see figure 13. The ratio can be described as $r = \frac{\dot{Q}_{roof}}{\dot{Q}_{box}}$.

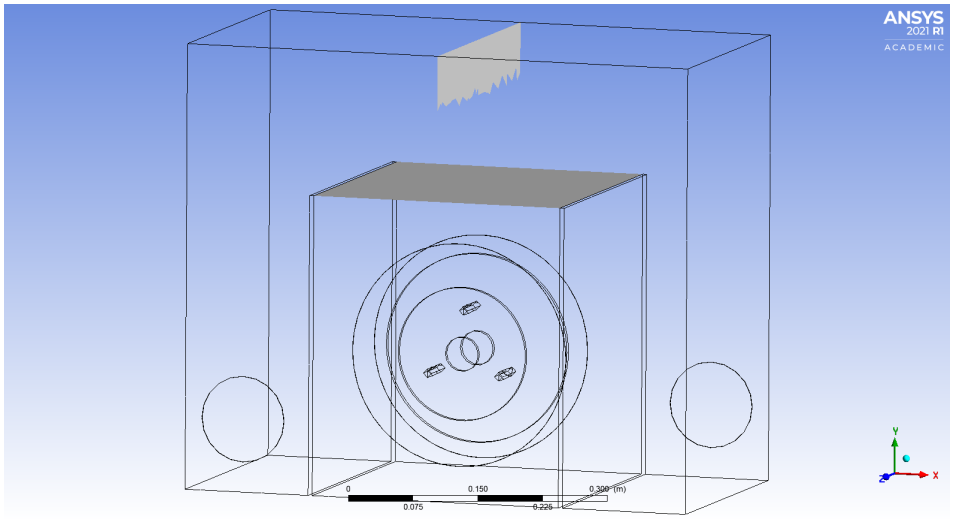

Figure 13: *Volume flow planes.*

Furthermore, a lid with an inspection hole is added. The inspection hole is set as a square with 100mm sides which can be seen in figure 14. The same meshing settings are used, with the addition of fine mesh sizing around the inspection hole. In total, 153786 elements and 30262 nodes makes up the mesh. The goal is to ensure mixing and interaction between the boxes.

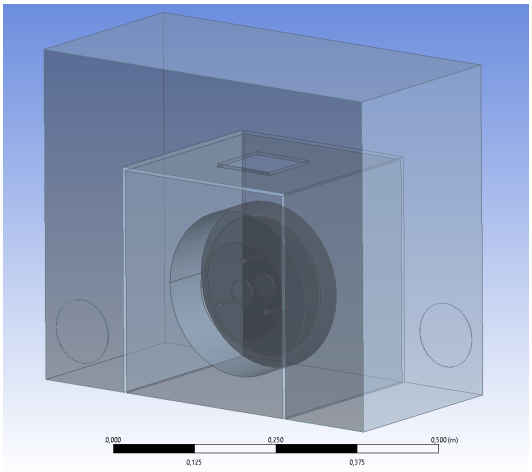

Figure 14: *Transparent geometry, 100mm square inspection hole.*

Finally, a lid with no inspection hole simulating a 5mm gap between the inner and outer box was evaluated. The mesh in close proximity to the gap was refined to see if there was any indication of airflow escaping the inner box. Figure 15 presents a skeleton view of the mesh, to clarify the fine gap the element size was set to 1.6mm and the outer mesh consisted of elements with the size of 30mm, resulting in a combined mesh of 497118 elements and 94151 nodes.

The mass flow through the different type of gaps were investigated. This could give an indication of how much particles are released. The mass flow was calculated for the three types of gaps by an expression which takes the air velocity times the gap area.

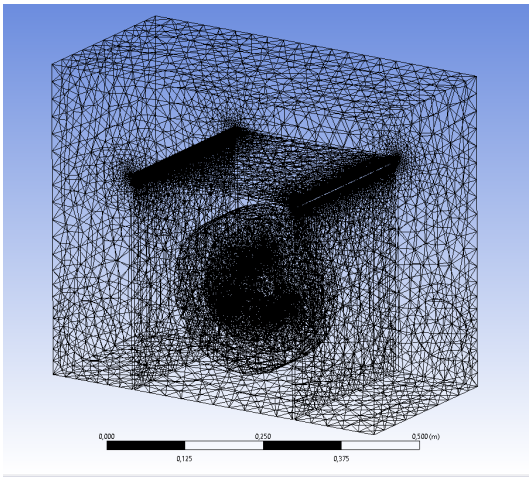

Figure 15: *Skeleton view of mesh, 5mm gap.*

Design of encapsulation

Taking inspiration from the system overview seen in figure 2 the encapsulation will be made in two stages. The first stage will encapsulate the clutch assembly, the second stage will encapsulate the first encapsulation and contain an inlet and outlet for particle sampling. The first stage will be sealed from the second stage in a way which represent a typical gearbox housing seal, the second stage will be sealed from the surrounding environment to ensure that all air entering the second stage have passed through the HEPA-filter.

The beams of the construction are made up by extruded aluminium profiles due to the practicality. The walls consist of acrylic glass to allow visual inspections for safety and educational purposes. The top lid of the inner box consists of an aluminium sheet instead of acrylic, due to the correlation with most modern engine to gearbox housing mating surface. Predominantly, this interface represent a real word scenario. It's possible to exaggerate the particles emitted from the case by opening a circular hole located in the aluminium top lid, which is convenient if the effect of gearbox inspection holes are to be investigated.

The distance measured from the aluminium top lid to the roof of the encapsulation is set of one design requirement, this is that the aluminium lid should be removable without disassembling the frame. The only part which needs to be removed if any changes is to be made to the seal is the acrylic roof of the encapsulation. This allows for easy access to the seal surface.

2.3.5 Data sampling

Temperature sampling

To ensure that the temperature of the clutch assembly is in its specified range, the temperature has to be sampled. This is done by a Pico Technology USB TC-08 data sampling tool and two k-type thermocouples. The thermocuples will measure the temperature inside the pressure plate 1mm from contact surface. Thermal paste is used to fill the holes and ensure that no thermal isolation can cause measurement errors.

To ensure that both pressure plates have the desired contact with the lamella, the temperature measurements are taken on both pressure plates. By sampling the temperature, it's easy to determine when the temperature have reached its steady state condition, since the derivative of the temperature as a function of time will be zero. It's also a good indication if the force from the springs has to be adjusted, in case of temperature imbalance or force magnitude error.

Rate of rotation

The angular speed is measured using a laser tachometer pointer. The laser is pointed against a machined piece of aluminium which is located on the rotating axle. This gives a direct measurement of the friction plate angular speed.

According to section 2.1.2, a normal to hard launch has a average slip speed difference of 100rad/s, which is the angular speed target. This is set by a combination of EM lever position and spring pretension. The friction coefficient, as mentioned in 2.1.2, is temperature-dependent which can cause the rotational speed to drop if the EM can't supply sufficient amount of torque. In a worst case scenario, initially a higher operating point has to be chosen and with time when the friction coefficient is changed with increasing temperature the desired operating point will be achieved.

3 Results

The results are divided into sections similar to methodology.

3.1 Frame

Figure 16 presents a CAD model of the modified frame. Four 6mm holes have been drilled which will be used to secure the encapsulation to the frame. An aluminium strut have been added to the frame, this strut will provide fastening points for the acrylic glass which will ensure that the inner box is fully sealed.

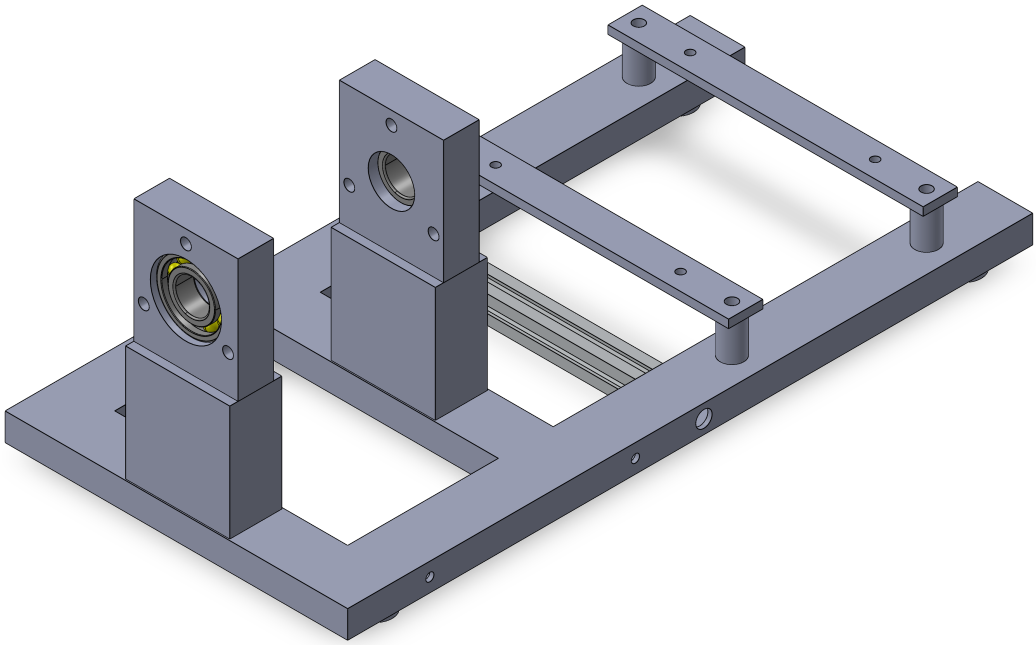

Figure 16: *Modified frame*

3.2 Clutch assembly

3.2.1 Pressure plate holder

Figure 17 presents the new pressure plate assembly including the spacers and slider pins. The original clutch cover have been removed and replaced by the pressure plate holder. The weight of the new pressure plate assembly is approximately half of the original one, resulting in less frictional losses and bending moment on the slider pins.

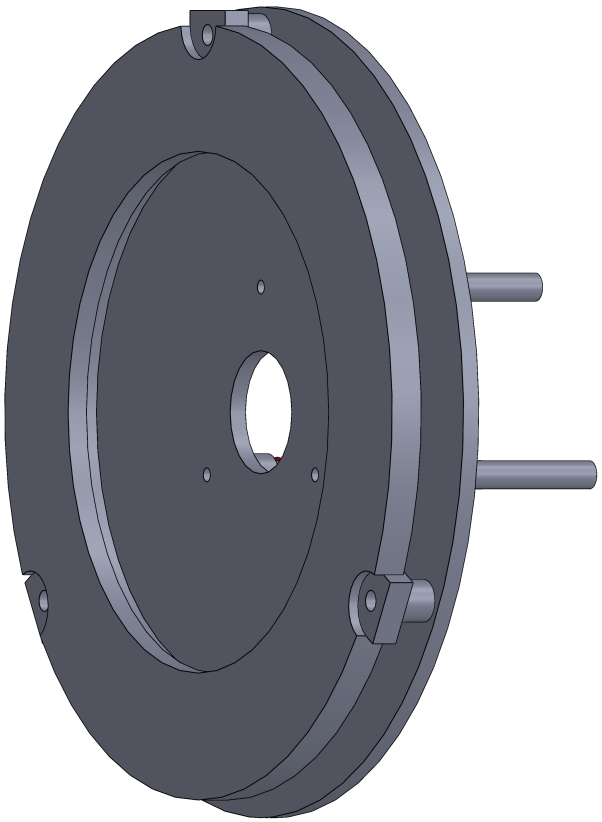

Figure 17: *Pressure plate holder including spacers and slider pins*

3.2.2 Friction plate shaft

Figure 18 presents a section view of the new friction plate shaft assembly, compared to the original shaft which utilizes the spline geometry the new shaft clamps the friction disc instead. The left shaft have a 6mm hole through its center and the right shaft is threaded, the threaded rod is inserted through the left shaft and screwed in to the right shaft, when the nut is tightened the shafts clamp the friction disc which makes it possible to transfer torque without using the spline geometry.

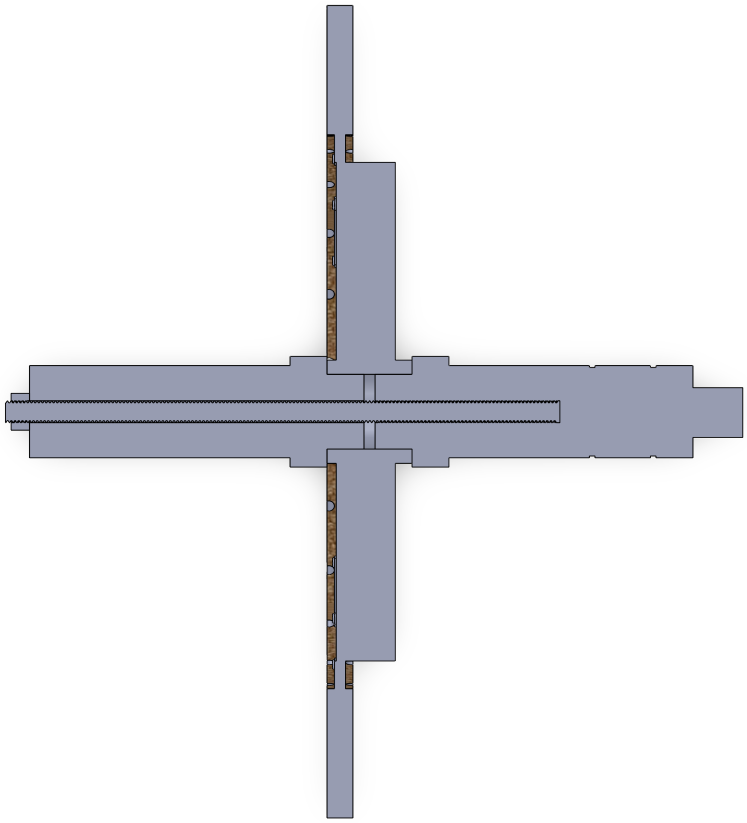

Figure 18: *Section view of the friction plate shaft assembly. The threaded rod and nut which clamps the two shafts together can be seen in this view*

3.2.3 Force application

Figure 19 presents a section view of the complete clutch assembly including the bearing holders. How placing a schim between the bearing holder and spring results in higher pretension is clearly seen in this picture.

Two snap ring grooves are also seen in this view, the snap ring groove located to the right of the right bearing is what locks the axial position of the shaft, there is also a second snap ring grove located to the left of the right bearing, however this is only necessary to use if the coupling type between the electric motor and the shaft is changed and doesn't lock the shaft to move right. As now the claw coupling locks the axial position to the right.

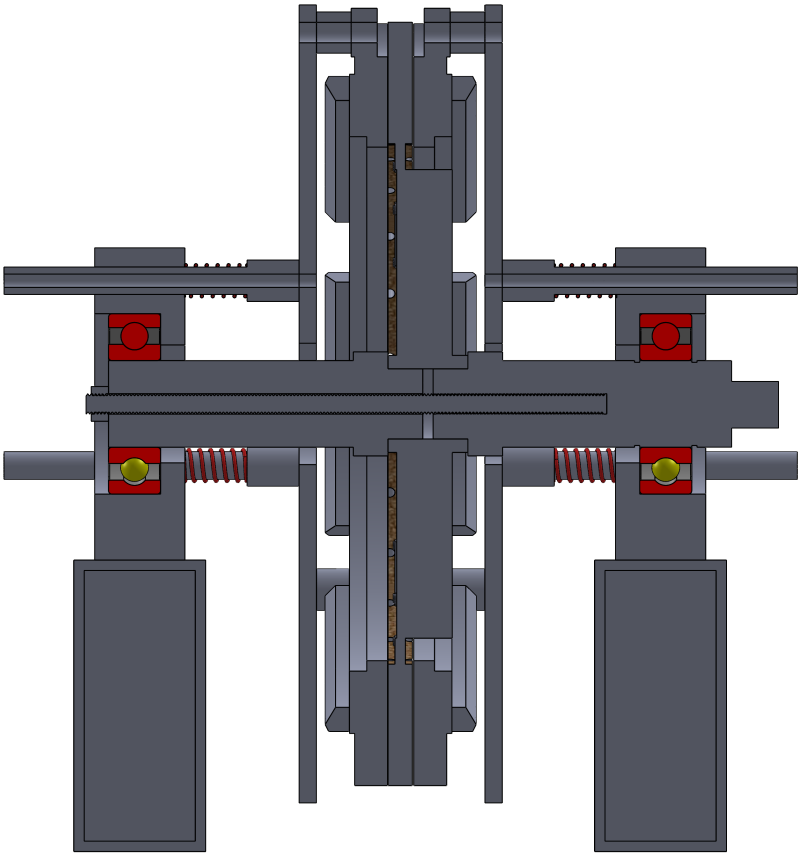

Figure 19: *Section view of clutch assembly.*

3.3 Electric motor

3.3.1 Thermal analysis

The result from the thermal simulation is presented in figure 20. The results point towards a peak temperature of 107°C, where the coldest spot is the aluminium pressure plate holder, which reaches 61°C.

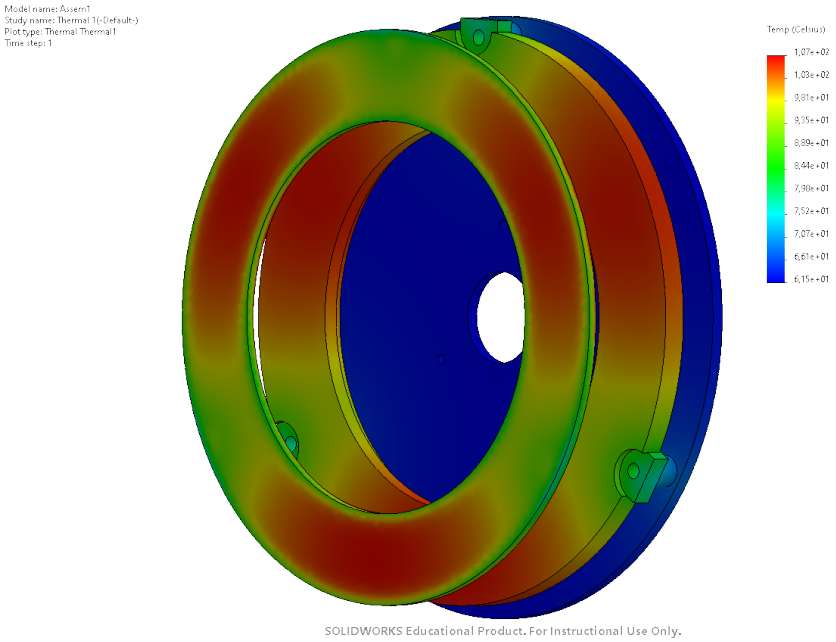

Figure 20: *Temperature distribution of friction and pressure plate.*

3.3.2 Speed-Torque diagram

The new Speed-Torque diagram for the maximum brush angle is presented in figure 21, this diagram was created by combining data from the original Speed-Torque diagram together with data points which was collected by using the symmetrical lever. This results in a new Speed-Torque diagram which covers the entire operating spectrum for the EM.

The maximum calculated torque which can be applied while containing the slip target of 100rad/s is 1.13 Nm, this condition is achieved when pretensioning the springs 2.5mm.

In table 4 the results for the calculated friction coefficient and input power is presented for three different pretensions. The maximum input power was calculated to 140 W and occurs at 1 mm pretension, the calculated friction coefficients indicate a decreasing trend with increasing contact pressure.

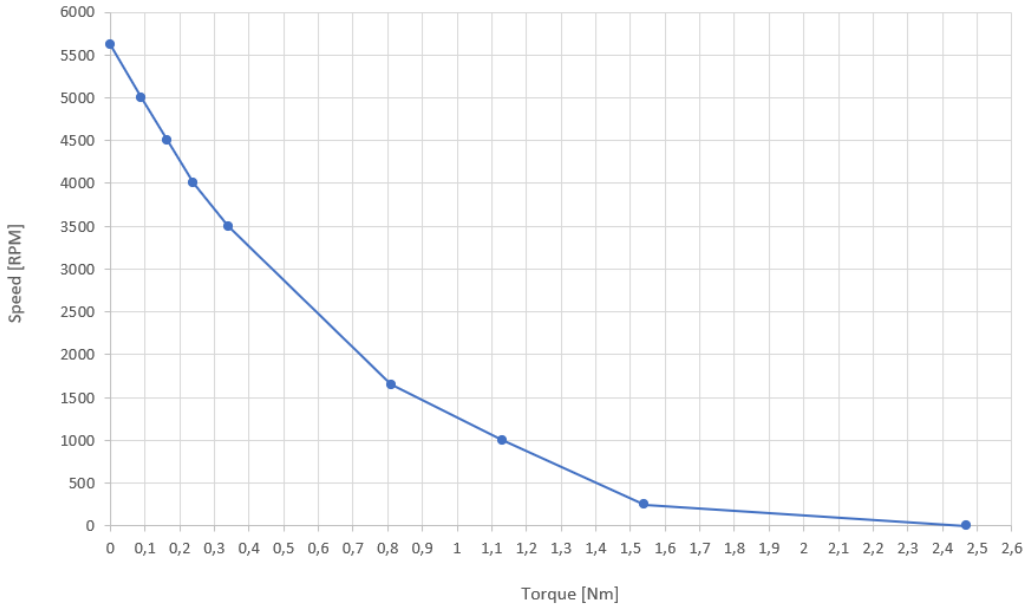

Figure 21: *Measured torque curve.*

Pretension [mm]	1	2.5	4	Max
Speed [RPM]	1650	1000	200	0
Torque static [Nm]	0.87	1.26	1.76	2.47
Torque dynamic [Nm]	0.81	1.13	1.54	-
Static μ	0.3	0.18	0.15	-
Dynamic μ	0.28	0.16	0.13	-
Power dynamic [W]	140	118	32	-

Table 4: *Measured and calculated data*

3.4 Temperature test

The temperature test was conducted in open air and the clutch was slipped for approximately 14 minutes, the resulting temperature curve is presented in figure 22. The front pressure plate represented by the blue curve is the one located closest to the EM, after approximately 13.5 minutes into the test the front pressure plate reached it's peak temperature of 76°C, the back pressure plate reached it's peak temperature at the same time stamp however the recorded peak temperature was 80°C.

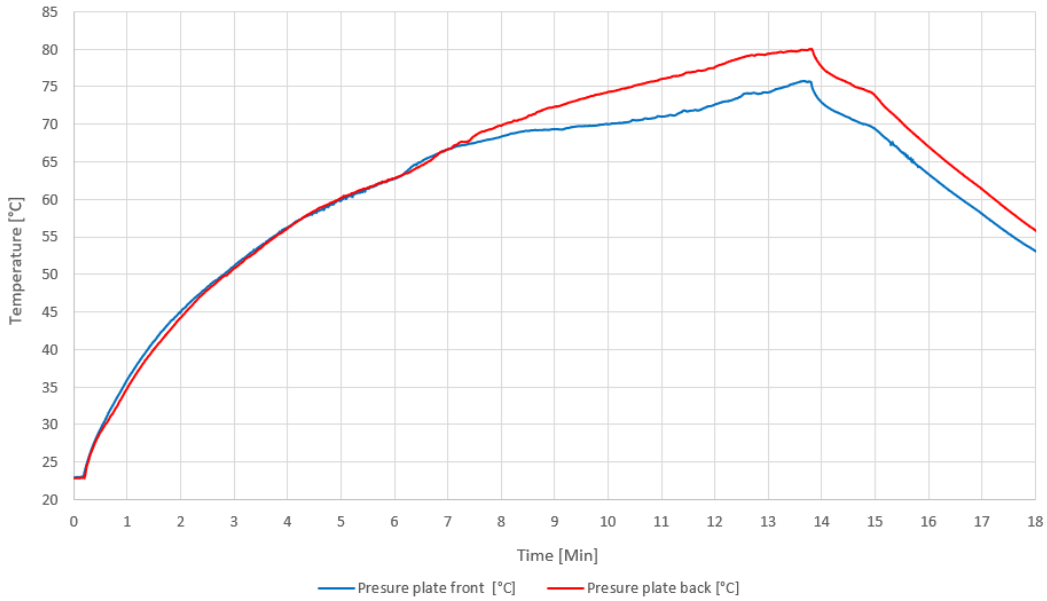

Figure 22: *Temperature vs. time, slip speed 100rad/s and 2.5 mm pretension.*

3.5 Encapsulation

3.5.1 CFD

The first simulation on the outer box indicates that the air is well mixed and provides a homogeneous outlet air mixture, including nanoparticles, if released. See figure 23. For the case of a 3m/s inlet speed, a average airspeed of 1m/s is observed inside the encapsulation.

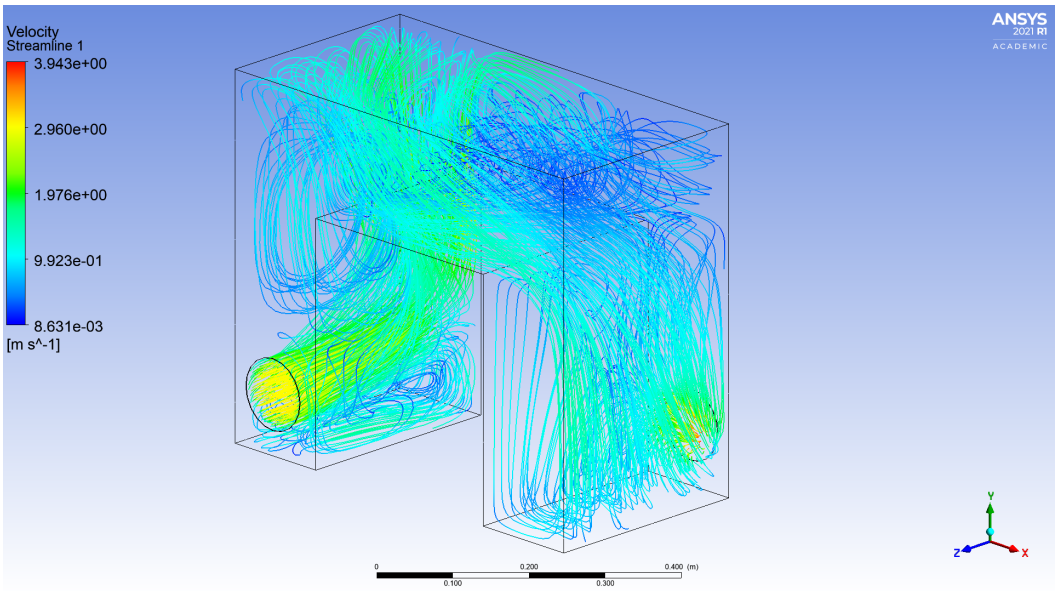

Figure 23: *Velocity streamlines, inlet in bottom left, outlet in bottom right.*

Adding the inner box together with the rotating friction disc but without a top lid, clearly indicates that the air does get affected by the rotating motion of the disc, see figure 24.

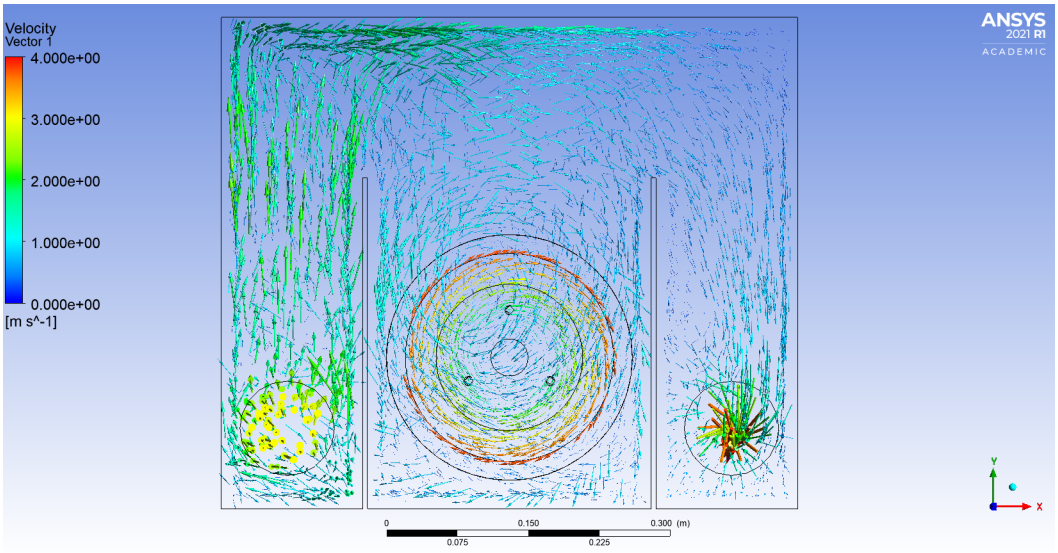

Figure 24: *Velocity vectors, no lid, inlet speed 3m/s.*

The swept airspeed cases are seen in figures 25, 26 and 27. The ratio r for the different inlet air speeds are in the order of rising speed, 1.22, 1.7 and 3.91. It's clear that the case for a inlet speed of 6m/s does show dense velocity vector along the top of the box, which indicates low entanglement and is confirmed by the large ratio r.

Comparing the case for inlet speed of 1m/s and 3m/s, it's seen that the airflow is mostly governed by the rotating friction plate and not the inlet air flow.

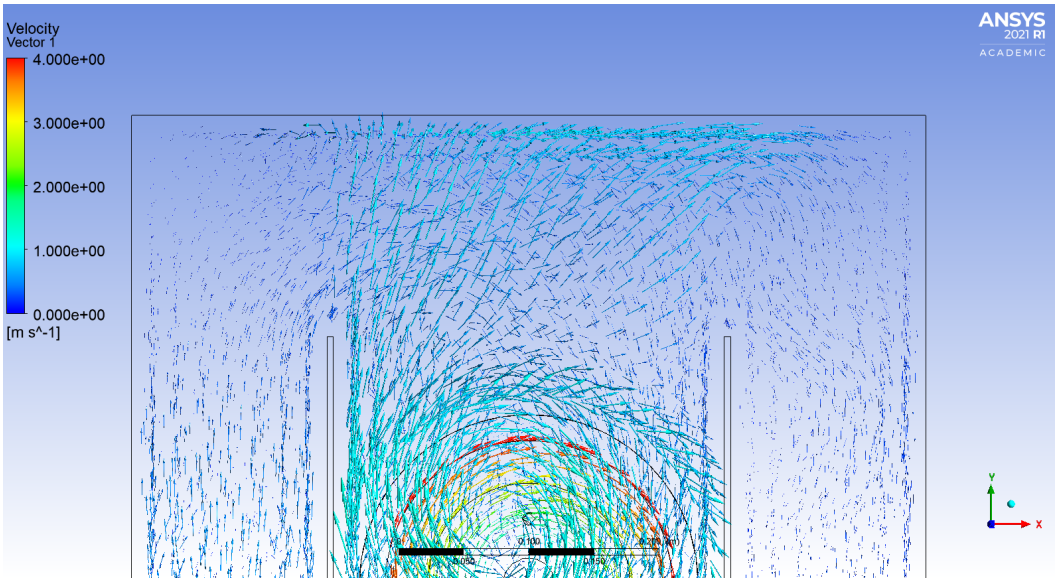

Figure 25: *Velocity vectors, inlet in bottom left, outlet in bottom right, inlet speed 1m/s.*

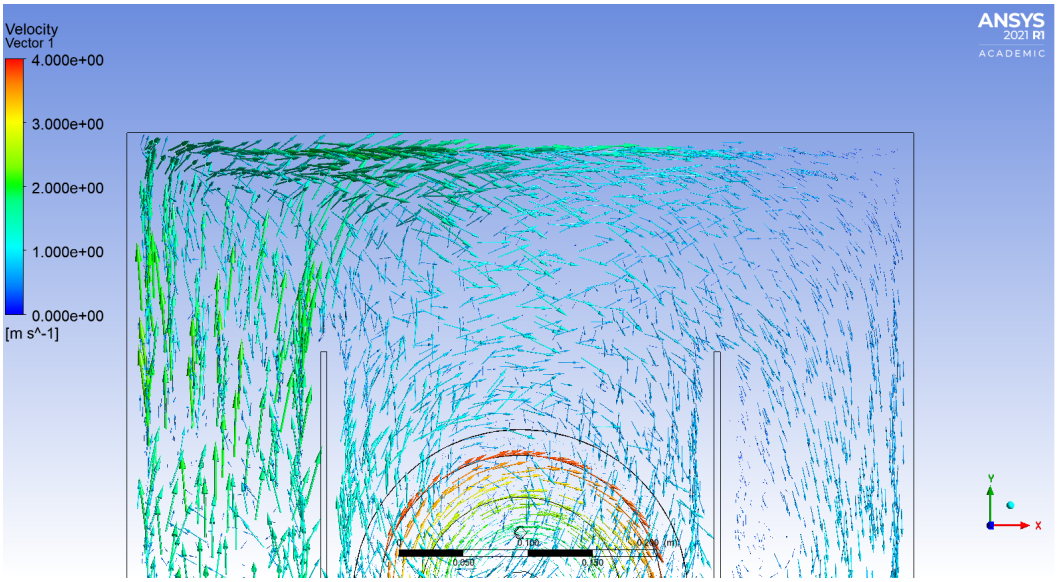

Figure 26: *Velocity vectors, inlet in bottom left, outlet in bottom right, inlet speed 3m/s.*

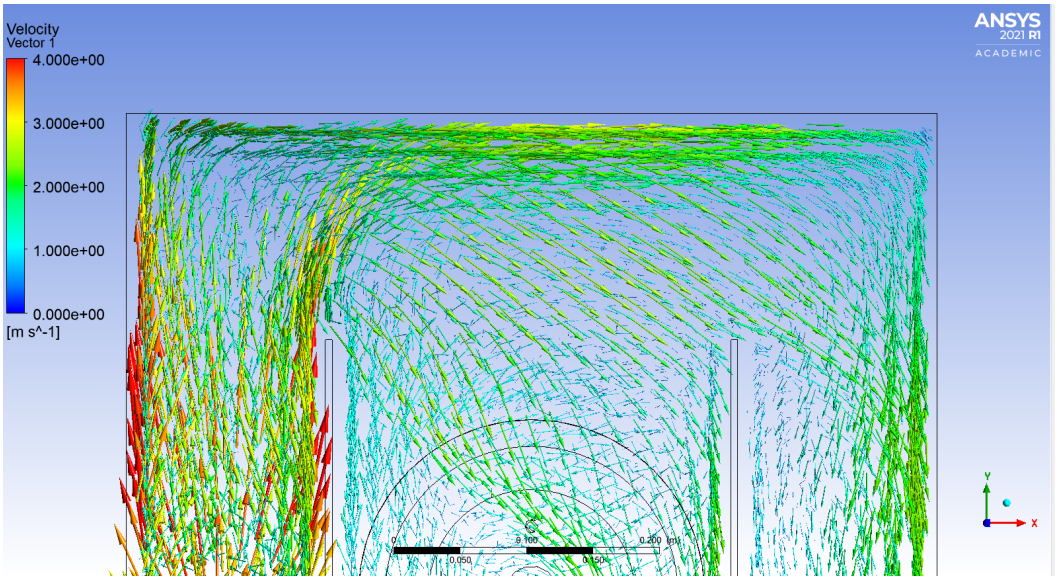

Figure 27: *Velocity vectors, inlet in bottom left, outlet in bottom right, inlet speed 6m/s.*

For the continuation of this section, the airspeed of 3m/s is chosen, reasons of which is explained in discussion section 4.5. For the chosen case, the air should pick up potential particles and transport them to the outlet sampling point. The result gives the confidence to continue with further limitations in the gap. The airflow through the inner box for an inlet speed of 3m/s was calculated to 0.87 $\frac{dm^3}{s}$.

The results with a square 100mm inspection hole and a lid with a 5mm gap are presented in figure 28 and 29. A limitation in the flow entering and exiting the inner box compared to the case without lid is seen. The airflow into the inner box with the square inspection hole is now limited to 0.046 $\frac{dm^3}{s}$, approximately a factor 19 less than the previous case.

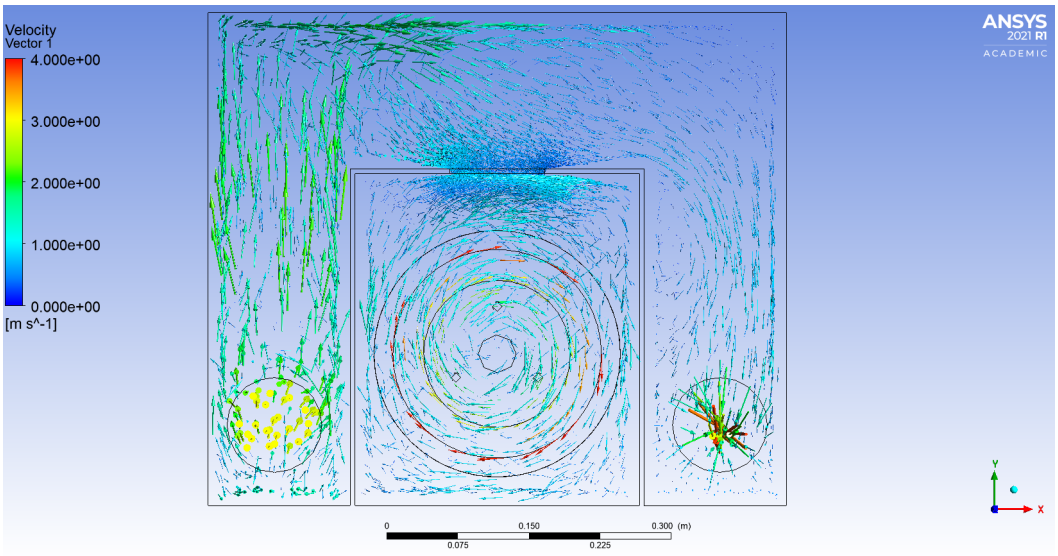

Figure 28: *Velocity vectors, 100 mm square inspection hole, inlet speed 3m/s.*

The results from the case with the 5mm lid gap are presented in figure 29. The flow has slightly decreased to 0.041 $\frac{dm^3}{s}$.

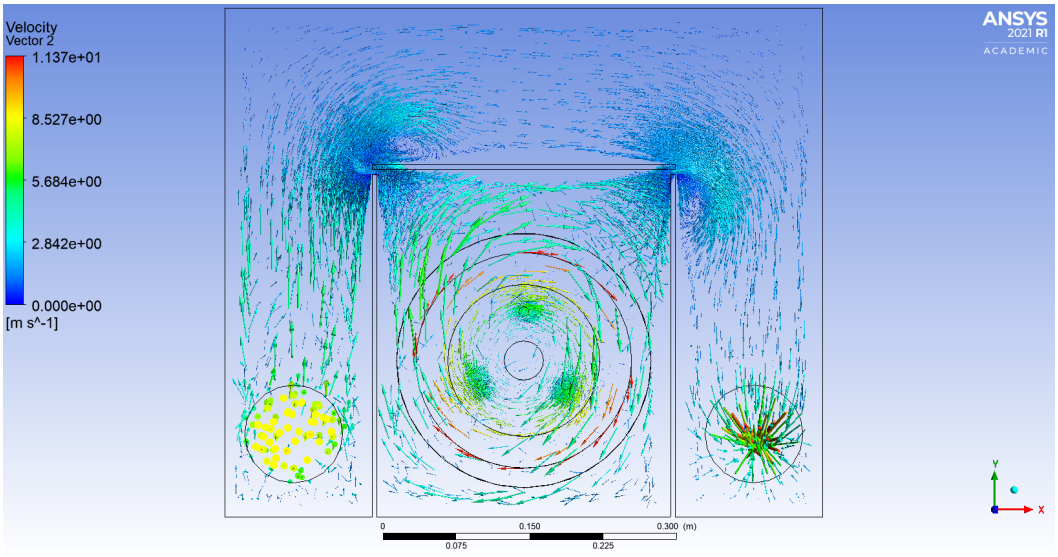

Figure 29: *Velocity vectors, 5mm gap, inlet speed 3m/s.*

It can also be seen in figure 30 that the desired airflow pattern is achieved. Most of the airflow enters at the gap closest to the inlet, and exits at close to the outlet. The colored contour describes the mass flow.

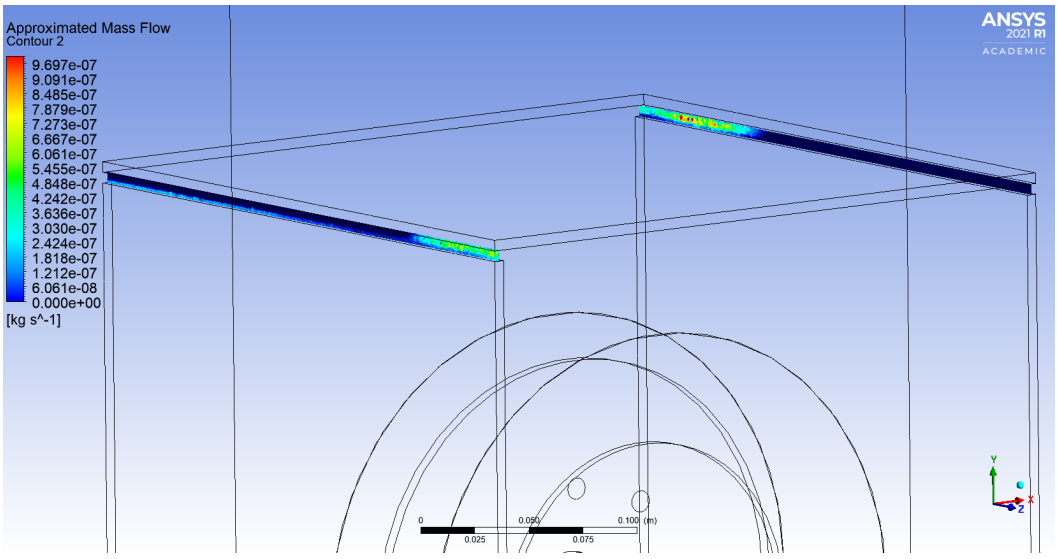

Figure 30: *Mass flow through the 5mm gap, inlet speed 3m/s.*

3.5.2 Design of encapsulation

Figure 31 presents the final design of the encapsulation excluding the acrylic glass. The inner box which encapsulated the clutch assembly measures 290[H] x 290[W] x 290[D] mm. These measurements ensures that the clutch assembly can be sealed in a secure way by utilizing the the frame and EM as fastening points. By choosing a small inner box volume similar to a transmission housing, enhances the possibility to direct the particles in to air streams and thereby possibly out to the second box.

The outer box which encapsulates the inner box measures 450[H] x 610[W] x 290[D], this allows some flexibility when choosing the inlet and outlet diameter which partly depends on the chosen fan, the maximum fan diameter in this case will be 140mm. The height between the aluminium lid and the roof of the box is chosen to 135mm, this allows the aluminium lid to be removed without disassembling the aluminium struts. If any inspection or correction is to be made on the clutch assembly, only the top acrylic glass has to be removed which in turn makes it possible to remove the aluminum lid.

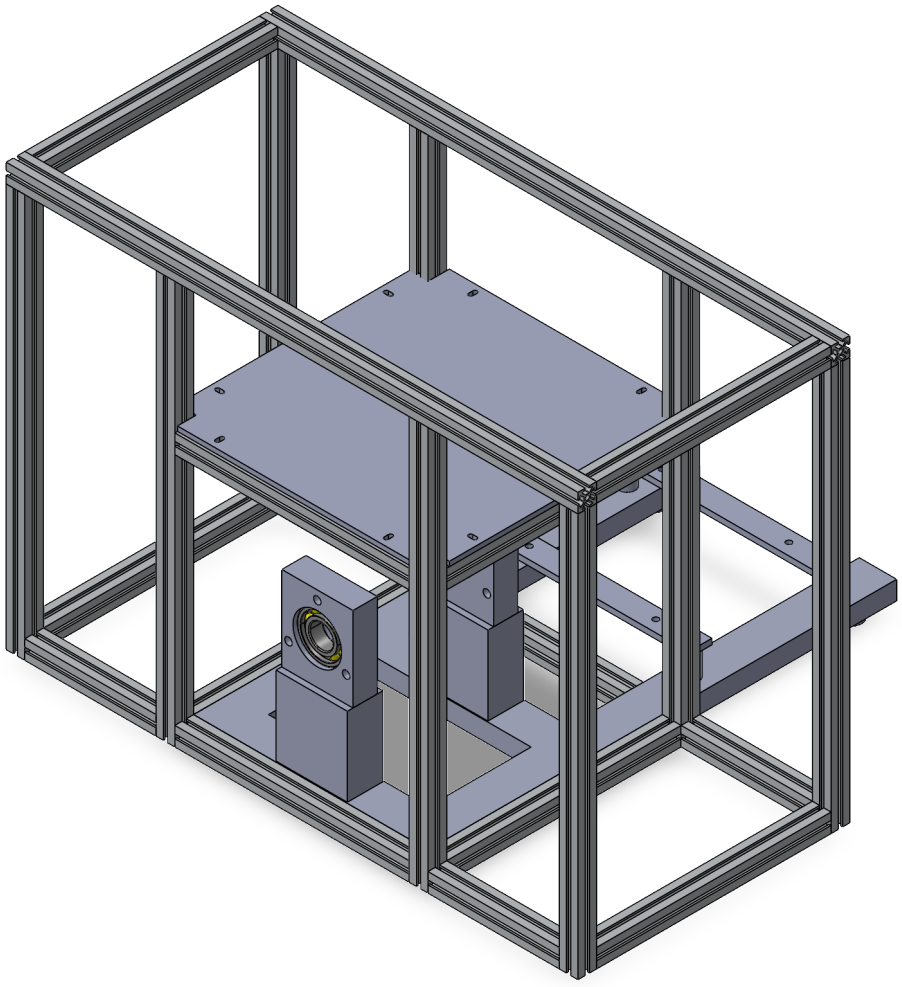

Figure 31: *Encapsulation and frame.*

3.6 Testing rig

Figures 32 - 35 presents the testing rig in multiple views.

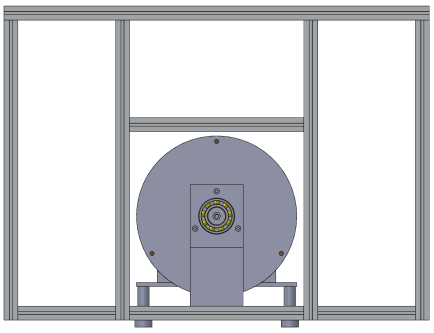

Figure 32: *Front view*

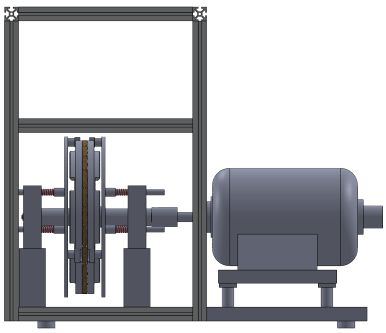

Figure 33: *Side view*

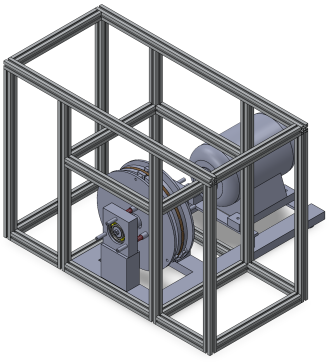

Figure 34: *Top view*

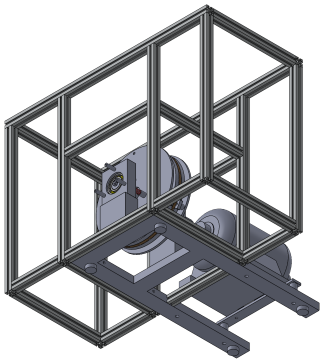

Figure 35: *Bottom view*

4 Discussion

4.1 Frame

The frame used in this thesis does fulfill the stated system requirements, the dimensions and shape of the frame made it possible to encapsulate the clutch in two stages. The frame also supports the clutch assembly and allows the springs to utilize the bearing holders for force application. The FEA integrity analysis indicated that the frame is well-dimensioned for the task and could be used together with a EM that can provide significant more torque. If other clutch models will be evaluated in the future and requires more torque input the frame itself could be reused without any modifications.

4.2 Clutch assembly

The chosen clutch model does fulfill the system requirements, as can be seen in appendix A section A2, there are large amount of vehicles models produced between 1997-2020 which potentially is equipped with this type clutch. Furthermore, the 220mm diameter of the organic friction plate and the possibility to separate the pressure plate from the clutch cover, made it possible to reduce the weight which resulted in a light and compact design.

Since the *constant slip* concept was chosen and as a consequence the required clamping force is low. Due to the ratio between the weight of the clutch assembly, and the axial force acting from the springs, there is a possibility that the contact surface between the friction plate and pressure plate is not fully sealed. One way to manage this is to increase the pretension of the springs to ensure that the entire pressure plate is in contact with the friction plate, with the current EM this is not possible since the necessary torque output from the motor is not sufficient enough and would result in a slip speed under 100rad/s.

A second option would be to improve the sliding operation of the pressure plates. The friction between the slider pins and bearing holder holes is as today unpredictable, one possible scenario is that drag generated from the friction for each slider pin is different which affects the applied axial force. Since the axial force applied is relatively small, the effect from the friction on the slider pins could impact the applied force quite substantially. Instead of relying on the sliding operation between the slider pins and bearing holders a solution which utilizes a bushing alternatively redesigning the sliding operation so it instead occurs between the pressure plate and the pressure plate holder would be preferred.

By utilizing a bushing between the slider pin and bearing holder, would result in uniform friction between all slider pins since the friction would be dependent on the bushing instead of the slider pin surface roughness. The more complex solution would be to move the sliding operation from the slider pins and bearing holders to the pressure plate and pressure plate holder. The bending forces on the sliding mechanism would decrease drastically and result in less friction compared to using the current slider pins, as now the slider pins have to carry both the bending forces and provide axial movement.

4.3 Electric motor

The Multifix MR 25 EM used in this thesis does fulfill the requirements in regards to the input power and speed control. The required clutch temperature range is reached while maintaining a slip speed of 100rad/s.

The thermal analysis gave a good indication of what temperature is to be expected. It's likely that the predicted temperature pattern from the thermal analyses will not be reached as shown, since the friction plate will be rotating and thus a homogeneous temperature is expected, at least for the friction plate. This means that the peak temperature should be slightly lower, but still within the requirements.

The results obtained from the testing of the EM shows some irregularities. One of these being the calculated power. According to the manufacturer the EM has a power output of 185W, however our results points towards a lower power output. This comes down the the method which was used to measure the torque output from the EM, while the static friction coefficient can be measured relatively easy the dynamic friction coefficient is dependent on both temperature and more importantly, slip speed. This makes it problematic measuring the actual torque output using our method. The friction coefficient shows a tendency to increase with both increasing slip speed and temperature, this indicates that the measured dynamic friction coefficient is likely to low which explains the low calculated power output. The calculated friction coefficients indicates that the friction coefficient is decreasing with increased contact pressure, this is in contrast to what was expected and are likely an effect caused by friction losses in the bearings. For low contact pressure the bearing losses will have an significant impact on the calculated friction coefficient, if the bearing losses are greater than 0.6 Nm the results are reversed.

The motor does not leave much room for improvement in terms of raising the clutch temperature to above an allowed friction material continuous maximum. A more powerful machine would be preferable, to rather set the test limitation on the friction material itself instead of the power input available. The varying of parameters is always appreciated when gathering data, where a potential data collection could consist of, for example, particles released as a function of temperature or contact pressure. This is not currently possible to an extent that could be wanted, however, it was not amongst the objectives to be so.

4.4 Temperature test

The maximum temperature recorded during the 14 min test run was approximately 80°C. It should be noted that the test where performed in open air, thus the ambient temperature is lower than the anticipated when encapsulated which results in greater heat dissipation. The temperature reached is still within the specified acceptable range. The test was aborted slightly before the clutch assembly had reached it's final temperature. The derivative of the temperature curve was not equal to zero, although there was a significant gradient change after 13 minutes in the range of 1 $\frac{^\circ}{min}$. This indicates that the power output from the EM is sufficient enough to raise and maintain the temperature of the clutch at the desired level.

Initially the temperature between the pressure plates is equal, however after 11 min into the test there is a slight deviation in temperature between the two pressure plates. Why this deviation occurs is not entirely clear, one likely reason which causes this phenomena is the asymmetry of the friction plate. This can lead to that one side experience more turbulence, and thus greater cooling effects. There is also a possibility that the applied force on each side of the friction plate is not equal when the friction plate is rotating, the shaft which holds the friction plate in place is self centered by the forces from the springs, however the shaft can creep since the snap ring which locks the axial position allows for this by design. If we assume that the temperature is proportional against the input power in the range between 76-80°C a 0.04 mm offset of the shaft will result in a temperature difference of 4°C.

The importance of using thermal paste to avoid thermal isolation when sampling temperature data is shown in figure 36. The rear pressure plate represented by the red curve, had no thermal paste applied between the thermocouple and the pressure plate which resulted in a temperature deviation of approximately 20°C. To accurately sample temperature data the thermal paste should be be renewed if the thermocouples are removed from their sampling point, if not, there is a possibility that thermal isolation occurs which will lead to misleading temperature readings.

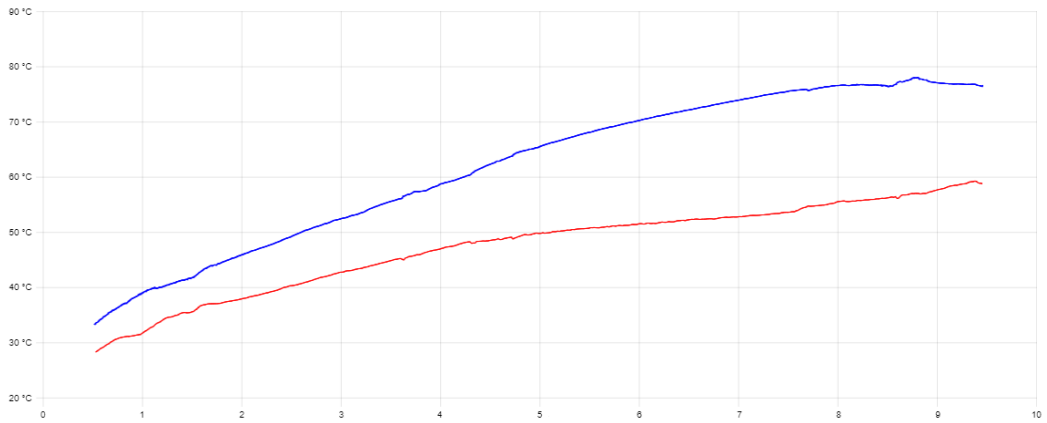

Figure 36: *Temperature error due to thermal isolation.*

4.5 Encapsulation

The outcome from the CFD-simulations which resulted in the encapsulation does fulfill the stated requirements. Due to the design of the encapsulation, it's simple to remove the entire encapsulation from the frame and changing the friction plate is estimated to take 15 minutes with the correct approach. Removing the bottom acrylic plate gives access to four screws which are used to hold the encapsulation to the frame, the screw which connects the friction plate shaft to the EM can also be accessed from here. When these five screws are removed, the whole encapsulation slides off the frame and there is full access to the clutch assembly.

After obtaining the results from the first simulation case, the confidence to continue with the chosen design is given. In the next step, the inlet airflow was evaluated. The case with an inlet velocity of 6m/s was promptly discarded due to the large ratio r. The inlet velocity is simply to high which causes the majority of the airflow to hit the roof of the encapsulation, this in turn leads to low entanglement since the majority of the air quickly exits the box.

The case with an inlet velocity of 3m/s was chosen based on the ratio r, but also after assessing the velocity vectors. This case gave us the most confidence when further constricting the flow from the rotating friction disc by adding a lid. The case with an inlet velocity of 1m/s did have the lowest ratio r but the flow around the gap area was considered worse than the 3m/s case. Therefore, the chosen inlet velocity is 3m/s and the following simulations were made based on that inlet speed.

Comparing the case with no lid against the case with an inspection hole, the air exchange rate is approximately 34 and 2 times per minute for the inner box, respectively. This implies that if particles are released from the clutch, the probability of being transported in a reasonable short amount of time to the sampling point is high. If we instead compare the inspection hole with the 5mm gap, we have approximately $\frac{2}{3}$ less area into the inner box, but only $\frac{1}{10}$ less volume flow. This indicates that the air does flow well around the gap. For the mechanical seal case, simulated by the 5mm gap, it's uncertain to draw any major conclusions. This is since the gap of interest is far smaller than the 5mm gap simulated. To be able to actually simulate the air through a such small gap data on surface roughness or seal type would be needed.

Only the surface that is mated against the ICE is considered as a leak source and thus only that crevice is considered. This might not be entirely accurate, since there is a potential pathway through the gearbox itself. Our judgement was that this route is far less likely, due to the gearbox being immersed in oil. Moreover, if one were to consider this pathway, the whole gearbox would have had to been included in the test environment, which adds a totally different complexity and changes the scale of the project.

4.6 Evaluation

4.6.1 Effect of clutch parameters

During normal clutch operation in a vehicle, the friction plate is eventually clamped with forces in the magnitude of thousands of Newton. One can then assume that the slip occurs at clamping forces substantially larger than what the friction plate in the designed testing rig is subjected to. For the purpose of this thesis, this effect works against the production of particles, which is one factor to consider when sampling.

The temperature of the friction plate in operation varies depending on which state the clutch is operating in. Since the elements surrounding the clutch operates in the vicinity of 90 °C, it's reasonable to assume that the operating temperature of the clutch reaches same temperature. Multiple rapidly succeeding engagements, which can occur in dense traffic, might raise the temperature to a critical level where wear is extensive and unpredictable. A combination of temperature and abrasive wear is then the major wear factor, compared to only regular abrasive wear which occurs at operating temperature.

4.6.2 Slip time

To be able to compare the slip time in the testing rig to a real scenario, the power input is considered. Hard launches as mentioned in section 2.1.2 can produce 35kJ of heat energy in the matter of three seconds. Assuming that 185W is induced into the testing rig clutch, it takes about 3 minutes of operation to simulate a hard engagement. It's assumed that a regular engagement induces one third of the energy compared to the hard engagement, thus one minute of slip is assumed to correspond to one engagement.

If the electric motor will be used to continuously slip the clutch at maximum brush angle from more than 15 minutes, extra precaution has to be taken. Due to it's low efficiency compared to other EM the temperature of the EM itself may be a concern, there is no maximum operating temperature stated in the technical documents provided by the manufacturer, the operator has to decide when to abort the test session and let the EM cool down.

4.7 Future work

To ensure that the no particles enters the outer encapsulating box through unintentional crevices a sealant should be applied between the acrylic glass and the aluminium struts. This would guarantee that all particles entering to box comes through the intentional crevices from the top plate.

The sliding operation of the pressure plates could be improved by using a bushing as discussed earlier. The temperature test was determined successful which indicates that the applied force from each pressure plate is near identical. If in a later stage a EM with a higher torque is used this will certainly not be necessary, however if the current EM will be used the testing rig could be refined using the proposed improvement.

Despite the fact that the electrical motor can deliver enough torque to slip and raise the temperature of the clutch to the desired temperature it has to be taken into account that according to the data sheet the motor was not designed to operate under these conditions. Because of this, there is a possibility that the life time expectancy of the motor is affected. To ensure reliability of the testing rig it should be considered to use a motor which is specifically designed to be used under the suggested conditions.

Contrary to what was originally planned, it's not possible to sample the rotational velocity of the friction plate. The Pico TC-08 data sampling tool have a maximum sampling rate of 10Hz which equals approximately 60rad/s. If it's determined in a later stage of the project that it's necessary to sample the rotational speed , this could be done by mounting a trigger-wheel at the end of the friction plate shaft which a hall-effect sensor triggers against. By choosing a similar device to the TC-08 one, which can sample and process a 5V signal at the desired frequency the rotational speed could easily be calculated and sampled.

5 Conclusions

The main objective of this thesis is fulfilled, while the targets were reached, the speed and temperature can be accurately controlled, while the potential emissions are captured. The inlet airflow is proposed to be close to but no more than $2.5\frac{dm^3}{s}$, which corresponds to a 100mm circulate inlet with an air velocity of 3m/s.

The design of the encapsulation has made it possible to change the friction disc without completely disassembling the testing rig. If multiple friction disc materials is to be tested it takes no more than 15 minutes to do a complete change of friction disc.

Despite the fact that there is a small temperature difference of approximately 3.9% between the pressure plates the temperature test was deemed successful. The minimum required temperature of 50°C is reached within 3 minutes and the steady state temperature of 80°C is reached after 14 minutes.

If the majority of the test sessions will require the friction disc to be slipped for more than 15 minutes continuously, and at the same time requires a minimum clutch temperature of over 80 °C, another EM with a power output of more than 185 W has to be used. The current EM will likely not be able to sufficiently raise the temperature above 80 °C for longer periods without the risk for overheating.

If the EM is operated at the maximum brush angle, based on the induced heat energy one minute of slip in the testing rig corresponds to a a normal clutch engagement, and three minutes of slip corresponds to a hard engagement.

References

[1] Theodoros Grigoratos and Giorgio Martini. Non-exhaust traffic related emissions. brake and tyre wear pm. Report no. Report EUR, 26648:7–9, 2014.

[2] P Monks, J Allan, D Carruthers, D Carslaw, G Fuller, RH OBE, M Heal, A Lewis, E Nemitz, M Williams, et al. Non-exhaust emissions from road traffic. Defra: Air Quality Experts Group, 2019.

[3] Michael G Jacko, Robert T DuCharme, and Joseph H Somers. Brake and clutch emissions generated during vehicle operation. SAE Transactions, pages 1813–1831, 1973.

[4] Marko Tirović. Dry clutch. Encyclopedia of Automotive Engineering, pages 1–30, 2014.

[5] Gearbox housing. `https://www.pngwing.com/en/free-png-tvzuv`. Accessed: 2020-06-10.

[6] Nanoparticle emissions from the transport sector: Health and policy impacts, Jun 2021.

[7] Mario Pisaturo and Adolfo Senatore. Simulation of engagement control in automotive dry-clutch and temperature field analysis through finite element model. Applied Thermal Engineering, 93:958–966, 2016.

[8] Xiaoliang Wang, Frank Einar Kruis, and Peter H McMurry. Aerodynamic focusing of nanoparticles: I. guidelines for designing aerodynamic lenses for nanoparticles. Aerosol Science and Technology, 39(7):611–623, 2005.

[9] Lars Vedmar. Transmissioner. KFS AB, 2007.

[10] Wikipedia. Clutch — Wikipedia, the free encyclopedia. `http://en.wikipedia.org/w/index.php?title=Clutch&oldid=1036549578`, 2021. [Online; accessed June-2021].

[11] Liang Yu, Biao Ma, Man Chen, Heyan Li, Chengnan Ma, and Jikai Liu. Comparison of the friction and wear characteristics between copper and paper based friction materials. Materials, 12(18):2988, 2019.

[12] Rydahls. Friction material RY258, 11 2017.

[13] Francesco Vasca, Luigi Iannelli, Adolfo Senatore, and Gabriella Reale. Torque transmissibility assessment for automotive dry-clutch engagement. IEEE/ASME transactions on Mechatronics, 16(3):564–573, 2010.

[14] Average age of the eu vehicle fleet, by country. `https://www.acea.auto/figure/average-age-of-eu-vehicle-fleet-by-country/`, February 2021. Accessed: 2021-05-06.

[15] 2019 (full year) europe: Best-selling car models. https://www.best-selling-cars.com/europe/2019-full-year-europe-best-selling-car-models/, February 2021. Accessed: 2021-05-06.

[16] Passenger car fleet by fuel type. https://www.acea.be/statistics/tag/category/passenger-car-fleet-by-fuel-type, February 2021. Accessed: 2021-05-06.

[17] Cubic capacity, average power. https://www.acea.auto/figure/cubic-capacity-average-power/, March 2018. Accessed: 2021-05-06.

[18] Abdul Jabbar N Khalif and IRAA Mousawi. Comparison of heat transfer coefficients in free and forced convection using circular annular finned tubes. Int J Appl Innov Eng Manag, 5:194–204, 2016.

[19] Classic ac motors: The repulsion-start induction motor. http://www.industrial-electronics.com/emct_2e_3k.html, August 2021. Accessed: 2021-08-13.

A Appendix

A.1 Frame FEA

Methodology

The load case and boundary condition are set as seen in figure 37. The material is mostly chosen as alloy steel, except the pressure plate holders which are made out of 6063 T6 aluminum , see apendix A section A3 for material properties. The maximum torque output from the EM was, as mentioned in section 2.3.3 measured to 2.5Nm, thus this was set on the EM shaft. The torque is equally distributed between the bearing holders. The bottom plate of the frame was fixated. The EM was set as rigid, since only the load on the frame is of interest. A simple mixed mesh was set, with 93651 nodes and 50239 elements, as seen in figure 38. The mesh consist primarily of tetrahedral elements.

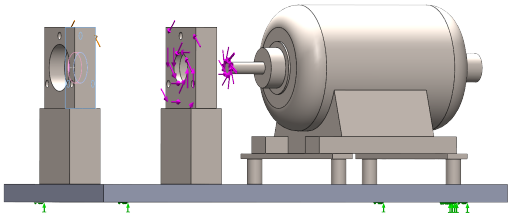

Figure 37: *Frame load case.*

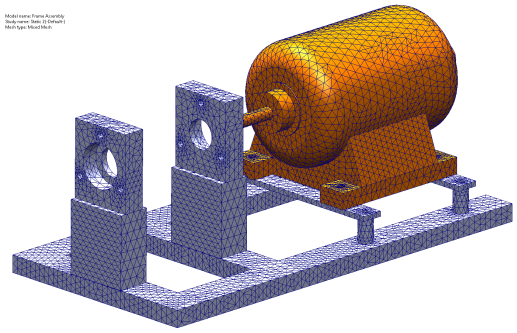

Figure 38: *Frame mesh.*

Moreover, an analysis was made with focus on the pressure plate holders including the slider pins, which is expected to be the weakest point in the construction. This mesh is as seen in figure 39, and consists of nodes 278929 nodes and 153874 elements. In this case, the load was instead placed on the pressure plate holders.

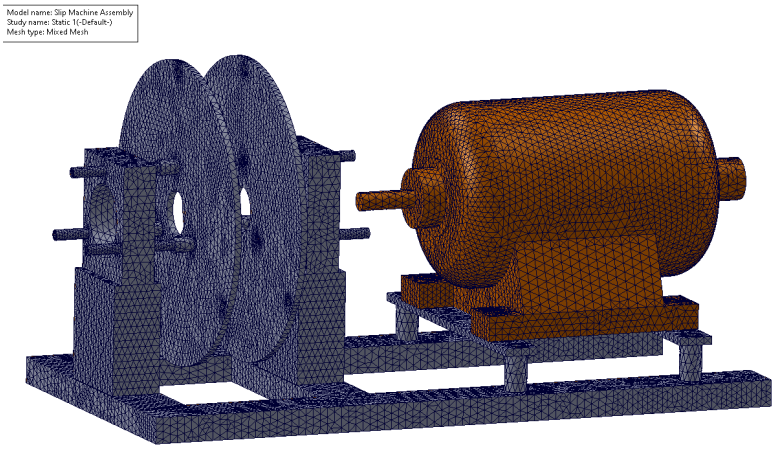

Figure 39: *Frame assembly, mesh.*

Results

The results from the static FEA analysis on the frame and assembly are presented in figure 40 and 41.

The maximum stresses for both cases are well within the yield strength limits of the materials used. For the first case, the maximum von Mises stress is 1.36MPa, with a material yield strength of 620MPa this results in safety factor of 455 for the frame.

In the case including the slider pins and pressure plate holders, the maximum von Mises stress is 3.72Mpa, again with a material yield strength of 620MPa this results in a safety factor of 166 for the slider pins.

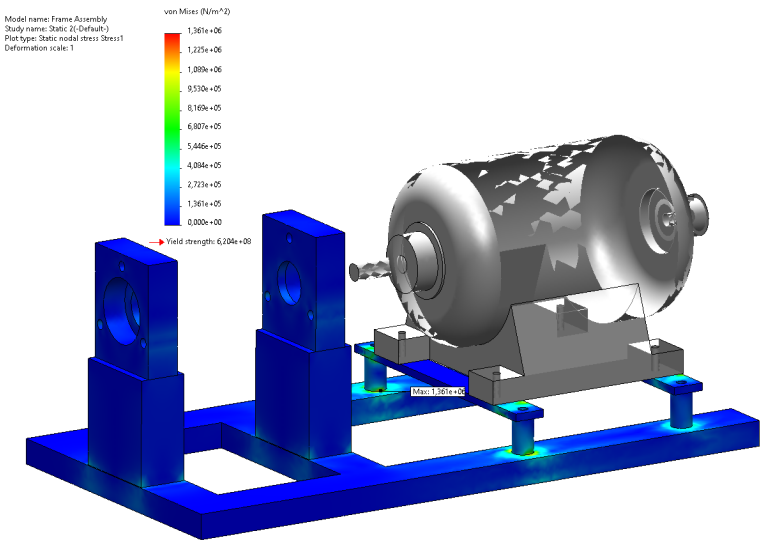

Figure 40: *von Mises stress for the frame, simplified.*

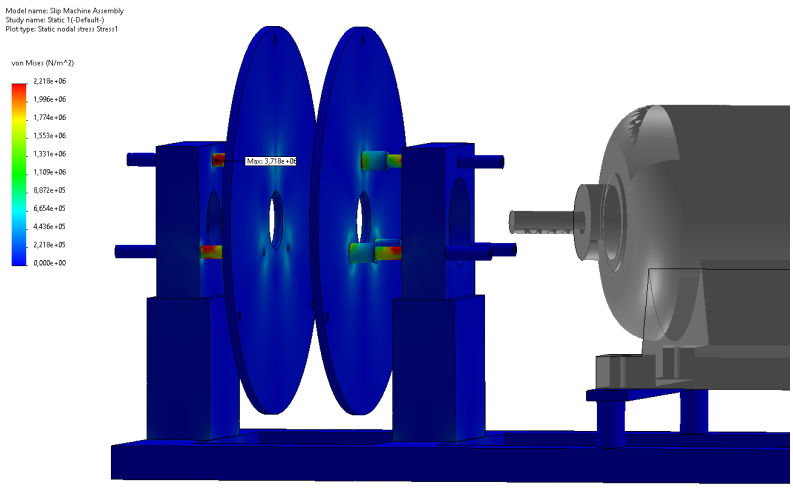

Figure 41: *von Mises stress for frame, including sliders and pressure plate holder.*

A.2 Clutch in cars

AUDI A1 (8X1, 8XK) (10-18)

AUDI A1 Sportback (8XA, 8XF) (11-18)

AUDI A2 (8Z0) (00-05)

AUDI A3 (8P1) (03-13)

AUDI A3 Convertible (8P7) (08-13)

AUDI A3 Sportback (8PA) (04-15)

SEAT ALTEA (5P1) (04-10)

SEAT ALTEA XL (5P5, 5P8) (06-10)

SEAT CORDOBA (6L2) (02-09)

SEAT IBIZA III (6L1) (02-09)

SEAT IBIZA IV (6J5, 6P1) (08-17)

SEAT IBIZA IV SPORTCOUPE (6J1, 6P5) (08-18)

SEAT IBIZA IV ST (6J8, 6P8) (10-16)

SEAT LEON (1P1) (05-13)

SEAT TOLEDO III (5P2) (04-09)

SEAT TOLEDO IV (KG3) (12-19)

SKODA FABIA I (6Y2) (99-08)

SKODA FABIA I Combi (6Y5) (0-07)

SKODA FABIA I Saloon (6Y3) (99-07)

SKODA FABIA II (542) (06-14)

SKODA FABIA II Combi (545) (07-14)

SKODA OCTAVIA II (1Z3) (04-13)

SKODA OCTAVIA II Combi (1Z5) (04-13)

SKODA RAPID (NH3) (12-19)

SKODA RAPID Spaceback (NH1) (12-19)

SKODA ROOMSTER (5J7) (06-15)

SKODA ROOMSTER Praktik (5J) (07-15)

SKODA YETI (5L) (09-17)

VW BEETLE (5C1, 5C2) (11-19)

VW BEETLE Convertible (5C7, 5C8) (11-19)

VW BORA (1J2) (98-13)

VW CADDY III Box (2KA, 2KH, 2CA, 2CH) (04-15)

VW CADDY III Estate (2KB, 2KJ, 2CB, 2CJ) (04-15)

VW CADDY IV Box (SAA, SAH) (15-20)

VW CADDY IV Estate (SAB, SAJ) (15-20)

VW EOS (1F7, 1F8) (06-15)

VW GOLF IV (1J1) (97-07)

VW GOLF IV Variant (1J5) (99-06)

VW GOLF PLUS (5M1, 521) (04-13)

VW GOLF V (1K1) (03-09)

VW GOLF V Variant (1K5) (07-09)

VW GOLF VI (5K1) (08-14)

VW GOLF VI Convertible (517) (11-16)

VW GOLF VI Variant (AJ5) (09-14)

VW JETTA III (1K2) (04-10)

VW JETTA IV (162, 163, AV3, AV2) (10-20)

VW LUPO (6X1, 6E1) (98-05)

VW PASSAT (3C2) (05-10)

VW PASSAT Variant (3C5) (05-11)

VW POLO (6R1, 6C1) (09-10)

VW POLO (9N) (01-14)

VW POLO Saloon (602, 604, 612, 614) (09-10)

VW TOURAN (1T1, 1T2) (03-10)

VW TOURAN (1T3) (10-15)

A.3 Material parameters

Property	**Alloy Steel**	**Aluminum 6063 T6**	**Friction material**	*Unit*
Elastic Modulus	210	69	0.2	GPa
Poisson's Ratio	0.28	0.33	0.3	$\frac{N}{A}$
Shear Modulus	79	25.8	-	GPa
Mass Density	7700	2700	1800	$\frac{kg}{m^3}$
Tensile Strength	0.723	0.24	-	GPa
Yield Strength	0.62	0.215	-	GPa
Thermal expansion coefficient	1.3e-05	2.34e-05	3e-05	$\frac{1}{K}$
Thermal conductivity	50	209	0.65	$\frac{W}{mK}$
Specific heat	460	900	1000	$\frac{J}{kgK}$